iScience

CellPress
OPEN ACCESS

Article

A CTGF-YAP Regulatory Pathway Is Essential for Angiogenesis and Barriergenesis in the Retina

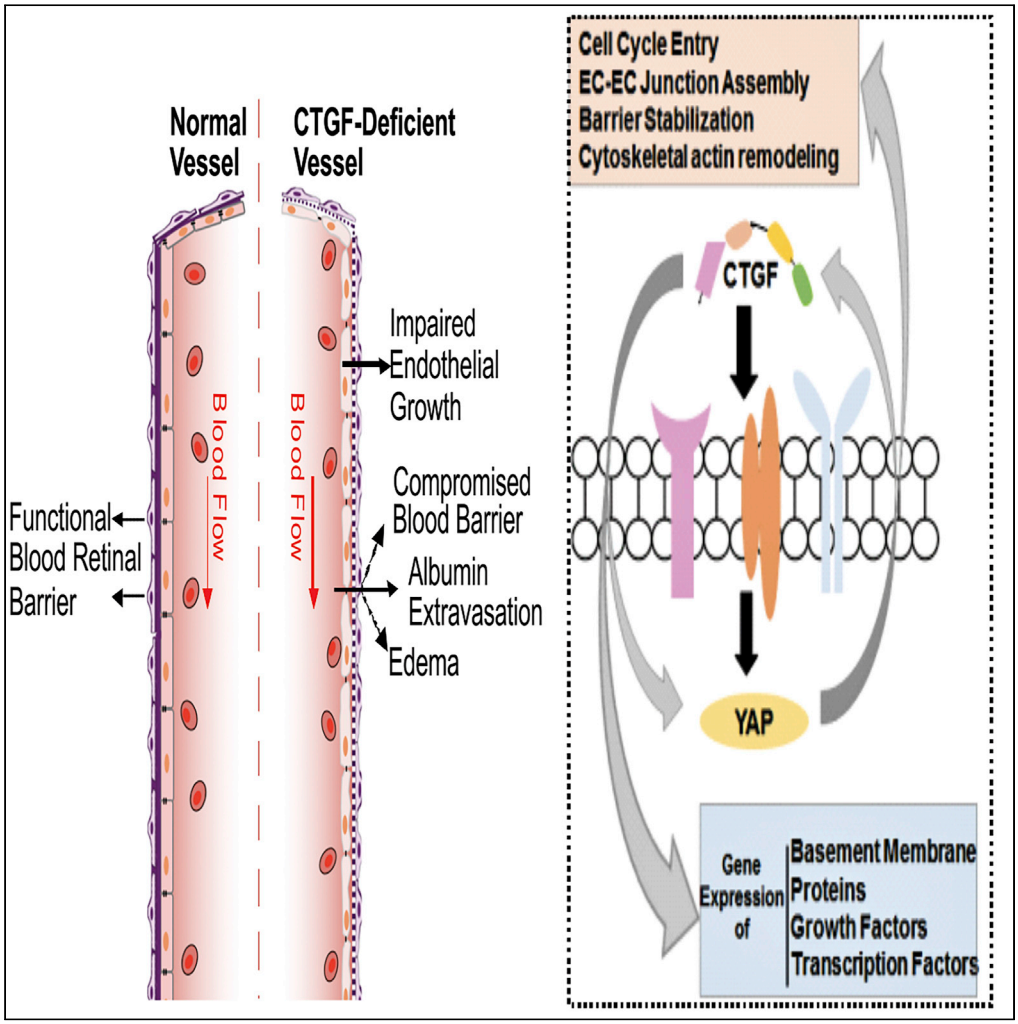

Sohyun Moon, Sangmi Lee, Joy Ann Caesar, ..., James A. Knowles, Jose Sinon, Brahim Chaqour

brahim.chaqour@downstate.edu, bchaqour@downstate.edu

HIGHLIGHTS

CTGF has a strong and persistent expression in the retinal vasculature

Mice lacking CTGF exhibit defects in angiogenesis and blood barrier integrity

CTGF-targeted genes include matrix, growth, and transcription co-factors like YAP

YAP re-expression partly rescues angiogenic and barriergenic defects of CTGF loss

Moon et al., iScience 23, 101184
June 26, 2020
https://doi.org/10.1016/j.isci.2020.101184

iScience

CellPress
OPEN ACCESS

Article

A CTGF-YAP Regulatory Pathway Is Essential for Angiogenesis and Barriergenesis in the Retina

Sohyun Moon,[1] Sangmi Lee,[1] Joy Ann Caesar,[1] Sarah Pruchenko,[1] Andrew Leask,[2] James A. Knowles,[1] Jose Sinon,[1] and Brahim Chaqour[1,3,4,5,*]

SUMMARY

Connective tissue growth factor (CTGF) or cellular communication network 2 (CCN2) is a matricellular protein essential for normal embryonic development and tissue repair. CTGF exhibits cell- and context-dependent activities, but CTGF function in vascular development and barrier function is unknown. We show that endothelial cells (ECs) are one of the major cellular sources of CTGF in the developing and adult retinal vasculature. Mice lacking *CTGF* expression either globally or specifically in ECs exhibit impaired vascular cell growth and morphogenesis and blood barrier breakdown. The global molecular signature of CTGF includes cytoskeletal and extracellular matrix protein, growth factor, and transcriptional co-regulator genes such as *yes-associated protein* (*YAP*). YAP, itself a transcriptional activator of *CTGF*, mediates several CTGF-controlled angiogenic and barriergenic transcriptional programs. Re-expression of *YAP* rescues, at least partially, angiogenesis and barriergenesis in *CTGF* mutant mouse retinas. Thus, the CTGF-YAP regulatory loop is integral to retinal vascular development and barrier function.

INTRODUCTION

Functional vascular networks form as a result of a well-coordinated series of angiogenic events regulating endothelial cell (EC) proliferation, differentiation, polarization, and gene programming to produce stable tubular structures with specific barrier properties (Chow and Gu, 2015; Zhao et al., 2015). In the retina, angiogenesis occurs during postnatal stages when ECs from the brain invade the optic nerve, emerge from it, and spread over and within the retinal neuroepithelium (Fruttiger, 2007). This angiogenic process is coordinated with the simultaneous formation of a blood-retinal barrier wherein the paracellular permeability between adjacent ECs and transcellular transport across ECs are tightly regulated by junctional protein complexes and transporter proteins, respectively (van der Wijk et al., 2019). Cells within the cohesive vascular wall have cadherin-based adhesions at cell-cell junctions and integrin-based focal adhesions to cell-extracellular matrix (ECM) contacts. ECM proteins, in particular, form a network of fibrillary and fibrous proteins and glycans that are critical for all aspects of vascular growth and regeneration (Bishop, 2015). ECM proteins provide both anchorage points to the cells and chemical cues for directional migration, morphogenesis, and stability. In addition, EC-ECM interactions contribute to the acquisition of EC barrier properties appropriate for the nervous system (Scott et al., 2010; Segarra et al., 2018). However, the diversity of both the matrisome components (which constitute >1% of the proteome) and the mechanisms controlling the synthesis, composition, and remodeling of ECM proteins is suggestive of an intricate level of complexity for the control of angiogenesis and barriergenesis (Bou-Gharios et al., 2004).

Connective tissue growth factor (CTGF) is a candidate ECM protein whose precise function in the vascular matrix is largely unknown. *CTGF* was originally isolated by differential screening of cDNA libraries prepared from HUVECs and NIH 3T3 fibroblasts (Ryseck et al., 1991). The protein was named CTGF because of its mitogenic activity vis-à-vis fibroblasts and cultured ECs. CTGF is also referred to as cellular communication network 2 (CCN2) by virtue of its multimodular and structural analogy to the CCN family of proteins (Krupska et al., 2015; Perbal et al., 2018). The primary *CTGF* translational product is a ~40-kDa protein that contains 38 conserved cysteine residues dispersed throughout four distinct structural modules. CTGF elicits its biological activities through binding to various cell surface receptors including integrin receptors, cell surface heparan sulfate proteoglycans (HSPGs), low-density lipoprotein receptor-related proteins

[1]State University of New York, Downstate Health Science University, Department of Cell Biology, 450 Clarkson Avenue, MSC 5, Brooklyn, NY 11203, USA

[2]University of Saskatchewan, College of Dentistry, E3338 HS - 105 Wiggins Road, Saskatoon, SK S7N 5E4, Canada

[3]State University of New York, Downstate Health Science University, Department of Ophthalmology, 450 Clarkson Avenue, Brooklyn, NY 11203, USA

[4]SUNY Eye Institute, SUNY Downstate Health Science University, 450 Clarkson Avenue, Brooklyn, NY 11203, USA

[5]Lead Contact

*Correspondence: brahim.chaqour@downstate.edu, bchaqour@downstate.edu

https://doi.org/10.1016/j.isci.2020.101184

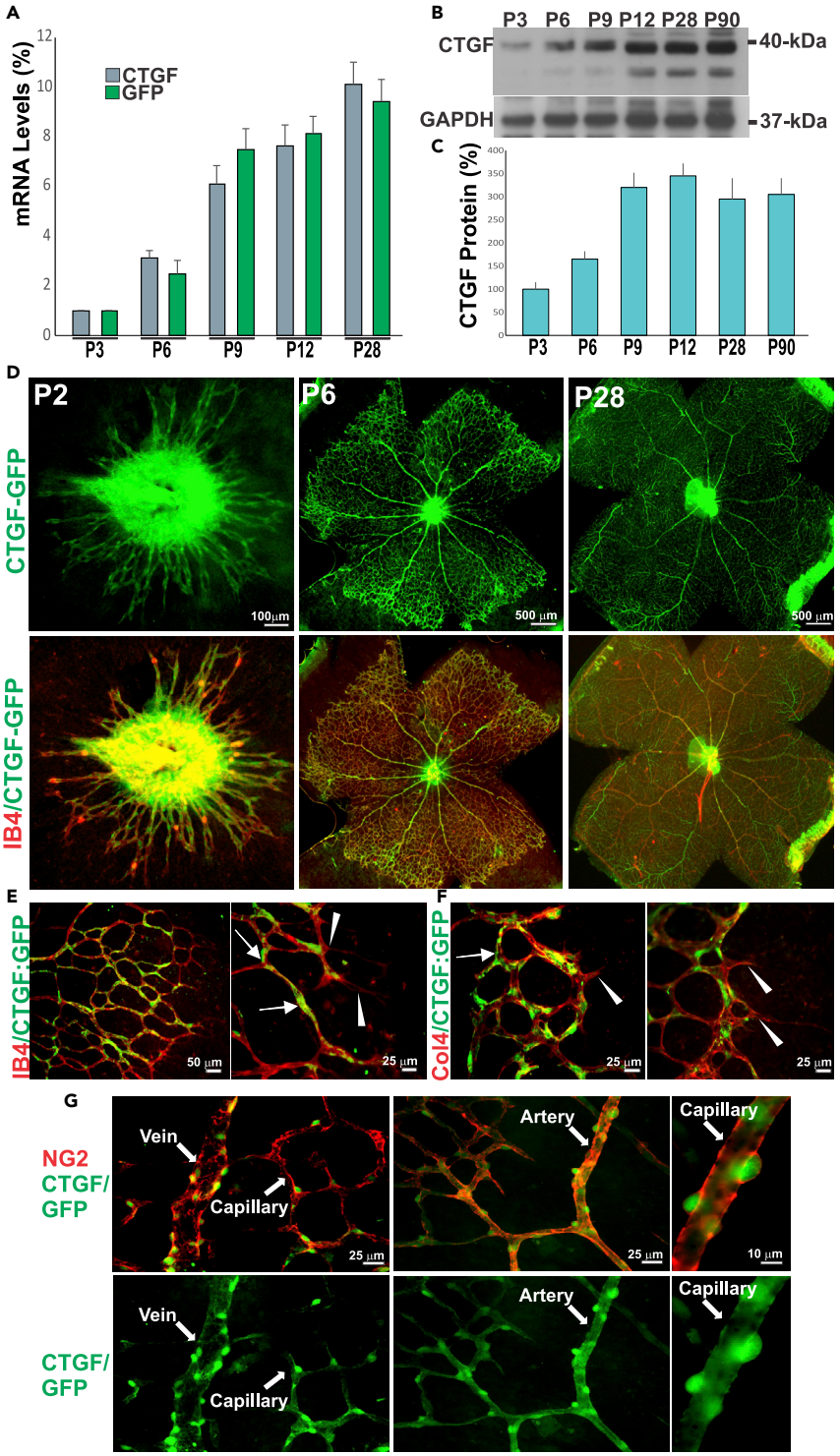

Figure 1. Expression and Cellular Localization of CTGF in the Postnatal and Adult Retinal Vasculature

(A) Analysis of *CTGF* and *GFP* transcript levels in the *CTGF:GFP* reporter transgenic mouse strain during postnatal development of the retinal vasculature by real-time PCR. *CTGF* and *GFP* mRNA levels were normalized to those of *GAPDH*. Data are means ± standard error (SE) (n = 4).

(B and C) (B) Analysis of CTGF protein levels in WT mouse retinas by western blotting. (C) CTGF protein bands were quantified by densitometric scanning. Error bars are SE of the means (n = 4).

Figure 1. *Continued*
(D) Unstained (upper panels) and IB4-stained (red) flat-mounted retinas of P2, P6, and P28 *CTGF-GFP* reporter mice. Merged images in the lower panels show IB4 colocalization with the CTGF:GFP signal.
(E and F) High-magnification images of retinal flat mounts of *CTGF:GFP* reporter mice stained with (E) IB4 and (F) Col4A1 antibody, respectively. Arrows and arrowheads indicate CTGF-GFP reporter signals in endothelial stalk cells and lack thereof in tip cells, respectively.
(G) NG2 marker expression in mouse retinal flat mounts. Note the colocalization of the CTGF:GFP signal with the NG2 marker in small arteries and capillaries.
See also Figure S1.

(LRPs), and TrkA in a cell type- and context-dependent manner (Gao and Brigstock, 2004; Lau, 2016). It was suggested that such interactions enable CTGF to regulate a variety of cellular functions including cell adhesion, proliferation, migration, differentiation, survival, and ECM synthesis. In addition, *in vitro* assays showed that the CTGF N-terminal and C-terminal moieties interact with glycoproteins, proteoglycans, growth factors, and proteases, although the *in vivo* significance of such interactions is not well understood (Dean et al., 2007; Hashimoto et al., 2002; Inoki et al., 2002; Pi et al., 2011). Global *CTGF* deficiency in mice demonstrated the importance of CTGF in cardiovascular and skeletal development, as *CTGF*-null mice exhibited defects in basic lung development and failed thoracic expansion, leading to perinatal lethality (Ivkovic et al., 2003). Although no overt vascular alterations were observed in *CTGF*-deficient mice during the initial formation of the primitive blood vessels, deficiencies in the endocrine cell lineage and reduced growth plate angiogenesis were noted. In adults, CTGF plays an important role in wound repair and CTGF protein levels correlate with many vascular and inflammatory diseases such as arthritis, diabetic nephropathy, and retinopathy (Chintala et al., 2012; Leask et al., 2002; Nguyen et al., 2008; Praidou et al., 2010; Tang et al., 2018). In a rat model of glomerulonephritis, *CTGF* levels were elevated in areas of crescentic extracapillary proliferation, periglomerular fibrosis, and interstitial foci (Gupta et al., 2000; Toda et al., 2017). Although these *in vivo* studies suggested a potentially important role of CTGF in physiological and pathological angiogenesis, the specific mechanisms whereby CTGF regulates blood vessel development and function remain to be investigated.

Here we provide the first evidence that CTGF directly regulates retinal tissue vascularization and blood barrier integrity. We show that the loss of *CTGF* function impairs a genetic angiogenic program involved in vessel sprout morphogenesis and branching and barrier integrity. We further provide data about exemplar CTGF target genes such as yes-associated protein (YAP), which when re-expressed in the vasculature, rescues, at least in part, transcriptional programs associated with *CTGF* deficiency. Our results shed light on the genetic landscape responsible for CTGF-dependent regulation of proper vessel formation and function.

RESULTS

Expression and Cellular Localization of CTGF in the Postnatal and Adult Retinal Vasculature

The retina is a complex neurovascular tissue organized into three cellular and two synaptic layers supported by a tripartite intraretinal vascular network. In mice, the retina is supported by three interconnected vascular layers that develop postnatally, making this model particularly useful for assessing the roles of genes potentially relevant to human vascular development and function (Lee et al., 2017). To determine the expression pattern and cellular sources of CTGF during retinal vessel development, we used a CTGF:GFP bacterial artificial chromosome transgenic mouse line in which the green fluorescent protein (GFP) reporter gene was placed downstream of a large *CTGF* promoter segment (>100 kb). Both endogenous *CTGF* and *GFP* transcript levels increased progressively as the superficial and deeper capillary plexuses invested the retina (Figure 1A). The dynamic *CTGF:GFP* expression pattern, which recapitulates endogenous *CTGF* transcript levels, suggests that the *CTGF* promoter-*GFP* reporter transgene contains the relevant *cis*-regulatory elements that regulate the *CTGF* gene *in vivo*. Similarly, CTGF protein levels progressively increased during retinal vessel development and plateaued during adult life (Figures 1B and 1C), indicating a constitutive expression of *CTGF* in the retinal tissue. We further examined the cellular sources of the CTGF:GFP signal in retinal flat mounts at P2, P6, and P28. As shown in Figure 1D, the reporter expression was found mainly in the expanding endothelial network stained with isolectin B4 (IB4) at P2 and P6 and persisted throughout the postnatal and adult periods. Further detailed analysis revealed a robust expression of *CTGF* in the ECs of the sprouting primary capillary plexus (Figure 1E). Endothelial tip cells with their filopodial extensions exhibited little or no CTGF:GFP signal (Figure 1F), whereas the trailing stalk

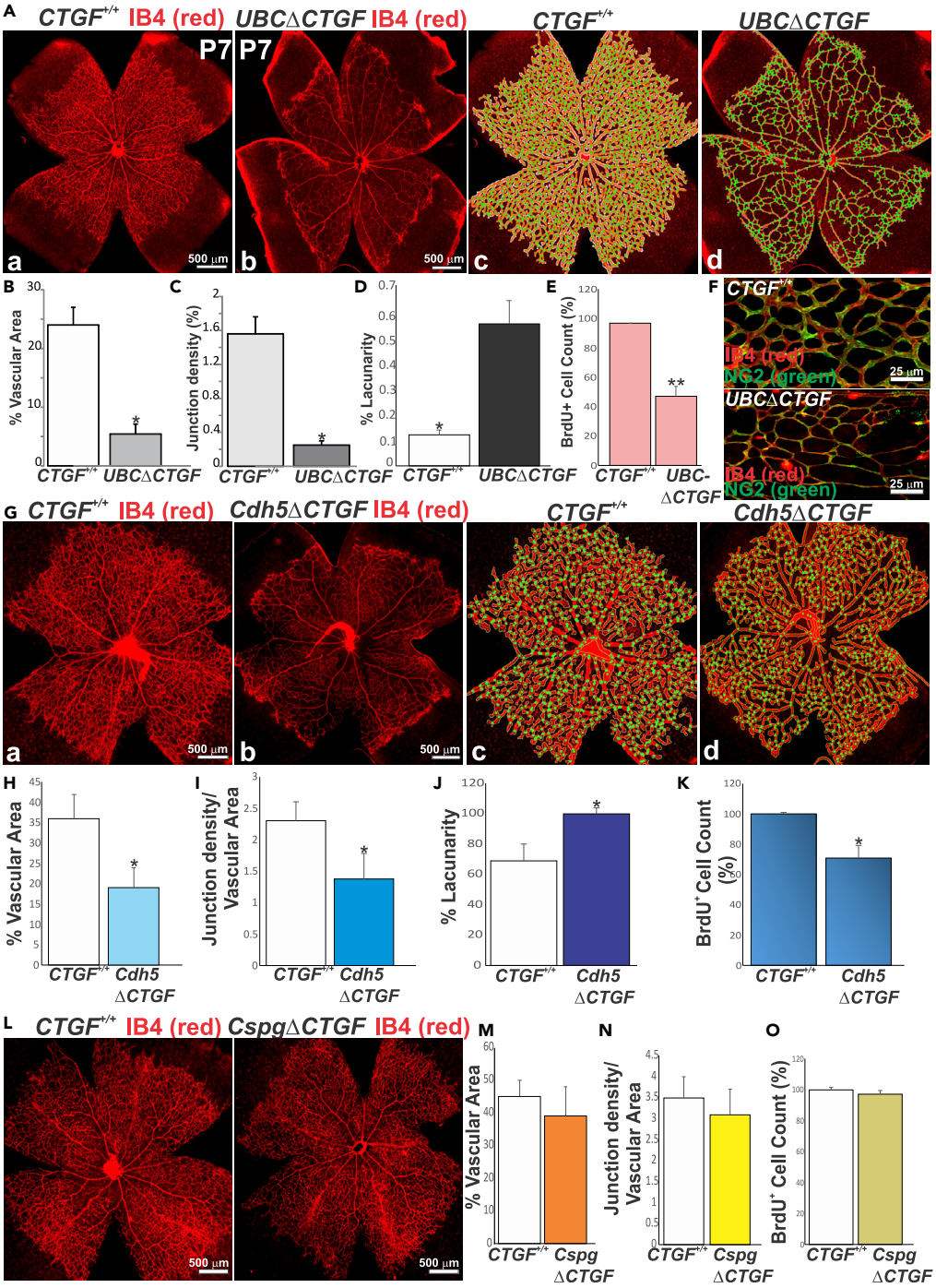

Figure 2. Loss of CTGF Function Altered Normal Vessel Growth and Morphogenesis

(A) IB4-stained whole retinal flat mounts of WT (a) and *UBCΔCTGF* (b) mice. Quantitative analyses of vascular parameters were performed with AngioTool software (c and d). The vasculature outline, skeleton, and branching points were denoted in white, red, and green, respectively.

(B–D) Graphical representations of the changes in (B) vascular area, (C) junction density, and (D) lacunarity between WT and *UBCΔCTGF* mouse retinas. *$p < 0.001$ versus $CTGF^{+/+}$ ($n = 5$).

(E) Number of $BrdU^+$ proliferating ECs per retinal area unit. **$p < 0.05$ versus $CTGF^{+/+}$ ($n = 5$).

(F) Representative immunofluorescence images of dual IB4 (red) and NG2 (green) staining of whole-mount retinas of $CTGF^{+/+}$ and *UBCΔCTGF* mice.

Figure 2. *Continued*

(G) IB4-stained whole retinal mounts of WT (a) and *Cdh5ΔCTGF* (b) mice and associated AngioTool-analyzed images (c and d), respectively.

(H–K) Graphical representations of the changes in (H) vascular surface, (I) junction density, and (J) lacunarity between WT and *Cdh5ΔCTGF* mouse retinas. $BrdU^+$ cell count in the WT and mutant mouse retinas is shown in (K). *$p < 0.05$ versus $CTGF^{+/+}$ ($n = 5$).

(L–O) Effects of pericyte-specific deletion of *CTGF* on the retinal vascular phenotype. Vascular parameters and proliferating cell counts were determined as described in (B–E).

See also Figure S2.

ECs showed a strong CTGF:GFP signal indicating that CTGF potentially regulates stalk cell function including proliferation, lumenization, and stabilization. In addition, as the vascular tree developed, the CTGF:GFP signal spread into neuron-glial 2 (NG2)-positive mural cells (i.e., pericytes) of small and large vessels. In the retina, despite their small caliber, differences in vessel diameter distinguish arteries/arterioles and veins/venules. NG2-positive mural cells of the retinal arteries and capillaries (Figure S1A) expressed the CTGF:GFP signal (Figure 1G). The larger veins similarly expressed the CTGF:GFP signal in their mural NG2-negative desmin-positive cells, but little to no *CTGF* expression appeared in venous ECs (Figure S1B). Moreover, detailed analysis of tissue cross sections revealed the CTGF:GFP signal in glutamine synthase $(GS)^+$ Müller cells and Iba-1^+ microglia, particularly those of the inner layer (Figures S1C and S1D). Expression of *CTGF* was not associated with astrocytes (data not shown), even though these cells are a major source of vascular endothelial growth factor (VEGF), a bona fide regulator of *CTGF* expression in cultured cells (Asano et al., 2019; Nakamura-Ishizu et al., 2012; Suzuma et al., 2000). The brain vasculature, which is similar in its complexity and properties to the retinal vasculature, exhibited a strong expression of the CTGF:GFP marker as well (Figure S1E). Thus, CTGF exhibits heterogeneous and spatiotemporal expression patterns during vessel morphogenesis and a sustained expression in the adult vasculature of the central nervous system.

Loss of *CTGF* Function Altered Normal Vessel Growth and Morphogenesis

As a secreted protein, CTGF exerts autocrine and paracrine actions because it localizes not only within the interstitial ECM but also pericellularly, due to its heparin-binding activity (Kireeva et al., 1997). To gain new insights into the function of vascular cell-derived CTGF, we examined the retinal vascular changes associated with global, EC-, or pericyte-specific loss of *CTGF* function. We used a *CTGF* mutant strain in which *loxP* sites had been engineered to flank exons 1 and 2 (Liu et al., 2011) (Figure S2A). These $CTGF^{flox/flox}$ mice were crossed with transgenic Cre mice bearing an inducible Cre recombinase under the control of the ubiquitin C (*UBC*), *Cdh5*, or *Cspg4* promoter to produce mouse mutants with global, EC-, and pericyte-specific deletion of *CTGF* (hereafter referred to as *UBCΔCTGF*, *Cdh5ΔCTGF*, and *CspgΔCTGF*), respectively (Figure S2B). The expression of *CTGF* was analyzed by qPCR to confirm its knockdown after three consecutive 4-hydroxytamoxifen (4HT) injections at P1, P2, and P3. *UBC*-, *Cdh5*-, and *Cspg4*-$CreER^{T2}$ recombination with floxed alleles effectively reduced *CTGF* mRNA levels by >85%, 55%, and 50% compared with wild-type (WT) (i.e., $CTGF^{flox/flox}$) mice, respectively (Figure S2C). CTGF protein levels were consistent with those of *CTGF* mRNA in WT and mutant mice (Figure S2D). The EC- and pericyte-specific knockdown was not fully penetrant due to the expression of *CTGF* by cells other than ECs and pericytes, respectively. The retinal vascular phenotypes were examined at P7 when the vasculature was not only still growing but also had acquired tissue- and barrier-specific properties to support organ function. Retinas from 4HT- or corn oil-injected littermate *UBC*-$CreER^{T2}$, *Cdh5(PAC)-CreER*^{T2}, and *Cspg4-CreER*^{T2} exhibited a vascular phenotype identical to $CTGF^{flox/flox}$ mouse retinas and were used as controls in all experiments. As shown in Figures 2A–2D, global loss of *CTGF* function resulted in a significant reduction of microvessel density, vascular branching, and vascular area. Arteriovenous differentiation and vascular expansion to the retinal edge were not affected, whereas the vascular network was partially shaped into rudimentary arterioles, venules, and capillaries. $BrdU^+$ cell count at the angiogenic front showed a 45% reduction of cell proliferation (Figure 2E). Pericyte coverage (normalized to vascular area) was unaffected in *UBCΔCTGF* mutant mouse vessels suggesting that *CTGF* loss had no apparent effect on mural cell recruitment to the vasculature (Figure 2F). Similar to global *CTGF* deficiency, EC-specific *CTGF* deletion induced a significant decrease in vascular area, branching points, and cell proliferation, and simultaneous increase of vascular lacunarity, although these alterations were slightly milder than those of the *UBCΔCTGF* mutants (Figures 2G–2K). Conversely, the retinal vasculature in mice with pericyte-specific deletion of *CTGF* (i.e., *CspgΔCTGF*) closely resembled that in the WT control with respect to vascular morphology, architecture, and density (Figures 2L–2O), indicating that pericyte-derived *CTGF* had no major effect on retinal vascular

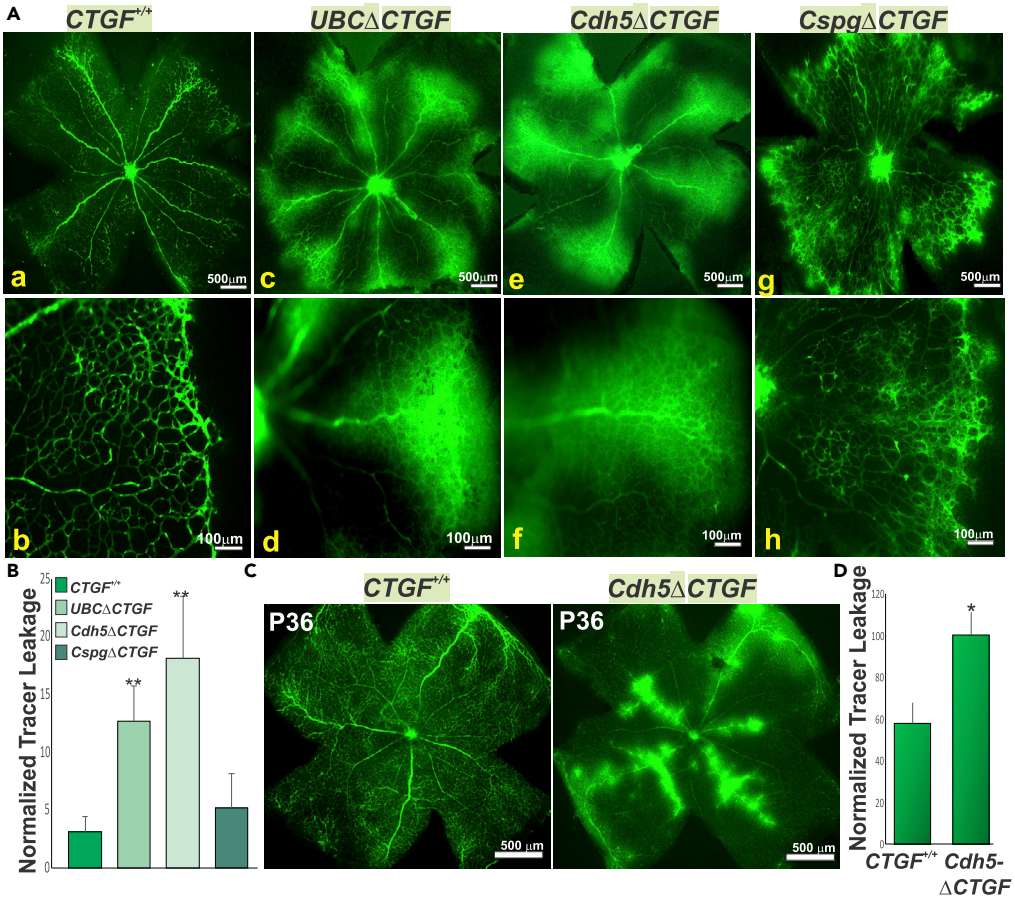

Figure 3. Loss of the Blood Barrier Function Following Global and EC-Specific Deletion of *CTGF*

(A) Retinal flat mounts from *CTGF*$^{+/+}$ (a and b), *UBCΔCTGF* (c and d), *Cdh5ΔCTGF* (e and f), and *CspgΔCTGF* (g and h) mice following retro-orbital injection of FITC-albumin. Note that the tracer remained confined to the vascular lumen in *CTGF*$^{+/+}$ and *CspgΔCTGF* mouse retinas. Note the hyperfluorescence of FITC-albumin in the retinal parenchyma as a result of FITC-albumin extravasation/leakage in *UBCΔCTGF* and *Cdh5ΔCTGF* mouse retinas.

(B) Vascular permeability index was normalized to total vascular area. ** p<0.05 *versus* *CTGF*$^{+/+}$.

(C) FITC-albumin-injected retinal flat mounts from *CTGF*$^{+/+}$ and *Cdh5ΔCTGF* adult (P36) mice that have received three consecutive injections of 4HT a week prior.

(D) Vascular permeability index measured as described in (B). Values are means ± SE (n = 3). Values in *Cdh5ΔCTGF* mice were set to 100% to facilitate comparisons among animals. *,p<0.05 *versus* *CTGF*$^{+/+}$.

See also Figure S3.

development. Thus, *CTGF* deficiency in the endothelium recapitulates, at least in part, the global loss-of-function phenotype.

Loss of Blood Barrier Function following Global and EC-Specific Deletion of *CTGF*

During vessel development, ECs tightly coordinate angiogenesis with vascular barrier formation. The latter involves the expression and engagement of tight junction (TJ) and adherens junction (AJ) proteins as well as expression of transporter proteins that limit paracellular and transcellular permeability between and across ECs (Dejana et al., 2008). To assess the effects of CTGF on barrier function, we examined the tissue localization of retro-orbitally-injected fluorescein isothiocyanate (FITC)-albumin, which does not traverse the vascular barrier under physiological conditions. In WT mice, the injected tracer was confined to the intravascular space of the retina (Figure 3A [a and b]). However, both *UBCΔCTGF* and *Cdh5ΔCTGF* mutant mice exhibited extensive vascular leakage, indicated by a diffuse hyperfluorescent background and patchy hyperfluorescence in the extravascular space (Figure 3A [c–f]). Conversely, pericyte-specific deletion of *CTGF* did not result in overt signs of FITC-albumin extravasation, which, in most cases, was similar to that of WT mouse retinas (Figure 3A [g and h]). Leakage of Evans Blue (EB), which rapidly binds to plasma albumin, was 4- to 9-fold higher in retinas of

*UBC*Δ*CTGF* and *Cdh5*Δ*CTGF* mutant mice, respectively, than that of WT controls (Figure 3B). There was no significant difference between WT and *Cspg*Δ*CTGF* mice with respect to EB leakage, which is consistent with the FITC-albumin results. Likewise, FITC-albumin extravasation was observed in the brain vasculature of the mutant mice indicating a defective blood-brain barrier as well (Figure S3A). Retro-orbital injection of Alexa Fluor 555-conjugated cadaverine, a small molecule (950 Da) reaching the size limit for passive paracellular transport through endothelial TJs, resulted in a remarkable infiltration of this tracer in the retinal and brain parenchyma of *CTGF*-deficient mice (Figures S3B and S3C). Thus, loss of *CTGF* function caused paracellular barrier disruption in the retina and brain. Furthermore, we determined whether the expression of *CTGF* is required for barrier maintenance by analyzing retinal vascular barrier permeability in adult (P36) mice following 4HT injection a week prior. As shown in Figure 3C, *Cdh5*Δ*CTGF* retinas showed numerous bright extravascular spots due to FITC-albumin leakage from the retinal vasculature. In contrast, age-matched littermates showed no tracer leakage in the retinal parenchyma. Vascular leakage index was 41% higher in *CTGF* mutant compared with age-matched WT retinas (Figure 3D), indicating the importance of CTGF signals in blood-retinal barrier maintenance as well.

Molecular Signature of *CTGF* during Retinal Vascular Development

The formation of an organized retinal vasculature depends on signaling among different vascular and non-vascular cellular components of the retina including ECs, mural cells, neurons, glia, and immune cells. As an ECM protein, CTGF signals may affect the interactions among all these cellular components. To determine the global genetic bases of CTGF-dependent regulation of vascular growth and barrier function, we examined the transcriptomic differences between $CTGF^{+/+}$ and *UBC*Δ*CTGF* mutant mouse retinas through RNA sequencing (RNA-seq)-based gene profiling. Following three consecutive 4HT injections from P1 onward, retinas from three different litters of $CTGF^{flox/flox}$ and $CTGF^{flox/flox}$-*UBC*-$CreER^{T2}$ intercrosses were harvested at P7 and processed for total RNA extraction and gene profiling. Unsupervised hierarchical clustering and principal-component analysis demonstrated clear segregation and reproducibility of the obtained gene expression profiles for WT and *UBC*Δ*CTGF* mutants (Pearson's correlation coefficient $\rho = 0.94$) (Figures S3A–S3C). The candidate CTGF-regulated genes encode proteins with a wide range of biological activities, likely reflecting the large diversity of cell types and circuits in the retina (Figure S4D). Genes that encode proteins for the biosynthesis of RNA, macromolecules, nucleobase-containing compounds, neurogenesis, and RNA polymerase transcription were highly differentially expressed between WT and mutant retinas.

To expand our RNA-seq data analysis beyond the initial cutoff parameters, which often are subjective, arbitrary, and biologically unjustified, we used gene set enrichment analysis (GSEA) to map all detected unfiltered genes to defined gene sets (e.g., pathways), irrespective of their individual change in expression (Subramanian et al., 2005). We identified 209 significantly changed genes (133 downregulated and 76 upregulated genes) in *UBC*Δ*CTGF* compared with $CTGF^{+/+}$ retinas (absolute $\log_2$ fold change >0.5, $p < 0.05$) (Figure 4A). When the normalized transcriptomic data were compared to 1,454 Gene Ontology gene sets in the GSEA Molecular Signatures Database (i.e., MSigDB) (Liberzon et al., 2015), 20 gene sets were significantly enriched in the $CTGF^{+/+}$ or *UBC*Δ*CTGF* group. Of these, 13 were closely related to neuronal progenitor differentiation linked to cone rod homeobox (CRX) pathway, cell cycle regulation (i.e., cyclins, p53, SRC, Kras), cell survival (i.e., Akt), and inflammation pathways (i.e., IL-15, NF-κB) (Figure 4B). Gene sets of the platelet-derived growth factor and mTOR pathways were similarly downregulated in *UBC*Δ*CTGF*. Other core-enriched differentially expressed genes were involved in the regulation of tip cell differentiation, angiogenesis, ECM, and ECM metabolic pathways (Figures 4C–4E). In addition, *CTGF* deficiency resulted in downregulation of angiopoietin 1, ROBO1, integrin β1, Slit-1, Ephrin B2, Ephrin Receptor B4, and Dll-1, and upregulation of integrin β1-binding protein 1 and thrombospondin 1. Downregulated ECM protein genes included laminin 4, elastin, secreted protein acidic and cysteine rich (SPARC), fibrillin-2, glypican 5, collagen 4A1, and tenascin-C, whereas vitronectin, Col17A1, Col16A1, and Col5A3 genes were upregulated upon *CTGF* deletion. Genes encoding growth factors such as insulin-like growth factor-I (IGF-I), pleiotrophin, opticin, LTBP-1, transforming growth factor (TGF)-β1, TGF-β2, and fibroblast growth factor (FGF)-10 were downregulated in *UBC*Δ*CTGF* mutant mice. These results are suggestive of an important role of CTGF in regulating angiogenesis-related processes such as cell growth, adhesion, migration and guidance, as well as cell-ECM interactions. Importantly, the expression of several transcriptional regulator genes (e.g., YAP, TEA domain [TEAD], NFAT5, and SRF) was downregulated upon loss of *CTGF* function. Transcription factors are endpoints of a network of signaling pathways enabling the cells to process signals they receive simultaneously from many different receptors. The multitude of transcription factors affected by *CTGF* deletion suggests that CTGF signals impact global mechanisms of gene regulation.

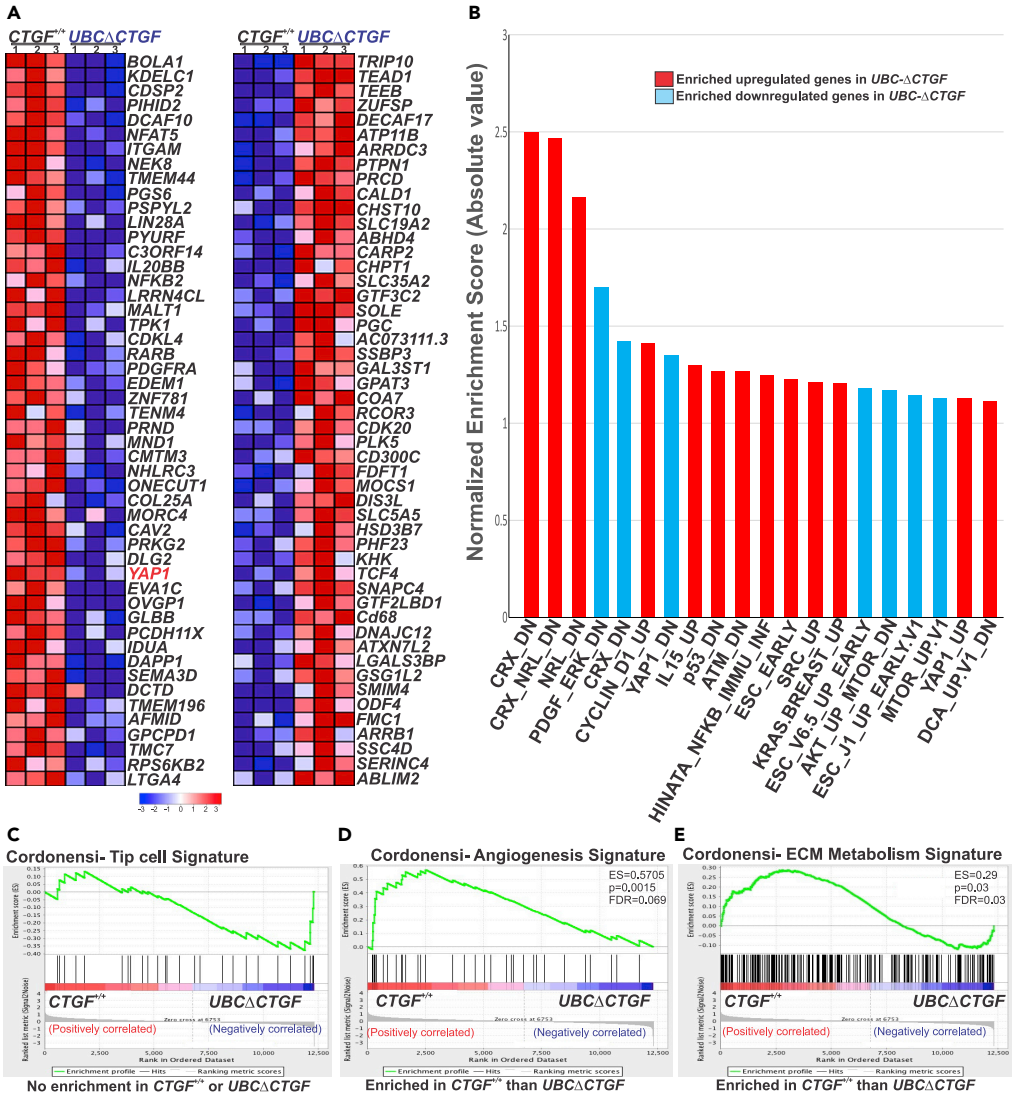

Figure 4. Molecular Signature of CTGF During Retinal Vascular Development

(A) GSEA-generated heatmaps of defined gene sets enriched at the top of a gene list ordered on the basis of expression differences between *CTGF*$^{+/+}$ and *UBCΔCTGF* mouse retinas. Range of colors (red to blue) indicates the range of expression values (high to low).

(B) Pathway enrichment analysis of differentially expressed genes in *UBCΔCTGF* versus WT mouse retinas. The clusters with functional terms that reached significance of $p < 0.05$ are shown. Online functional databases were used to extract each term.

(C–E) Enrichment plot of the gene set of (C) tip cell, (D) angiogenesis, and (E) ECM/cell adhesion pathways. Genes that appear before or at the peak are defined as core enrichment genes for that gene set. Genes whose expression levels are most closely associated with the *CTGF*$^{+/+}$ group are located at the left, whereas genes from the *UBCΔCTGF* gene set within the ranked list are located at the right.

See also Figure S4.

CTGF-Dependent Transcriptional Program Targets YAP Network Genes

YAP was among the most remarkable transcriptional regulators and key angiogenic factors that were differentially expressed as a result of *CTGF* deletion (Figures 4A and S2D). Like *CTGF*, *YAP* expression has been reported to increase in the retinal vasculature at an early stage of development (Choi et al., 2015; Neto et al., 2018). YAP is also required for the VEGF-VEGFR2 signaling axis that controls angiogenesis (Wang et al., 2017). VEGF-induced YAP activation leads to cytoskeletal remodeling, which orchestrates cellular decisions of proliferation, differentiation, cell shape, and polarity (Kim et al., 2017). To investigate the role of

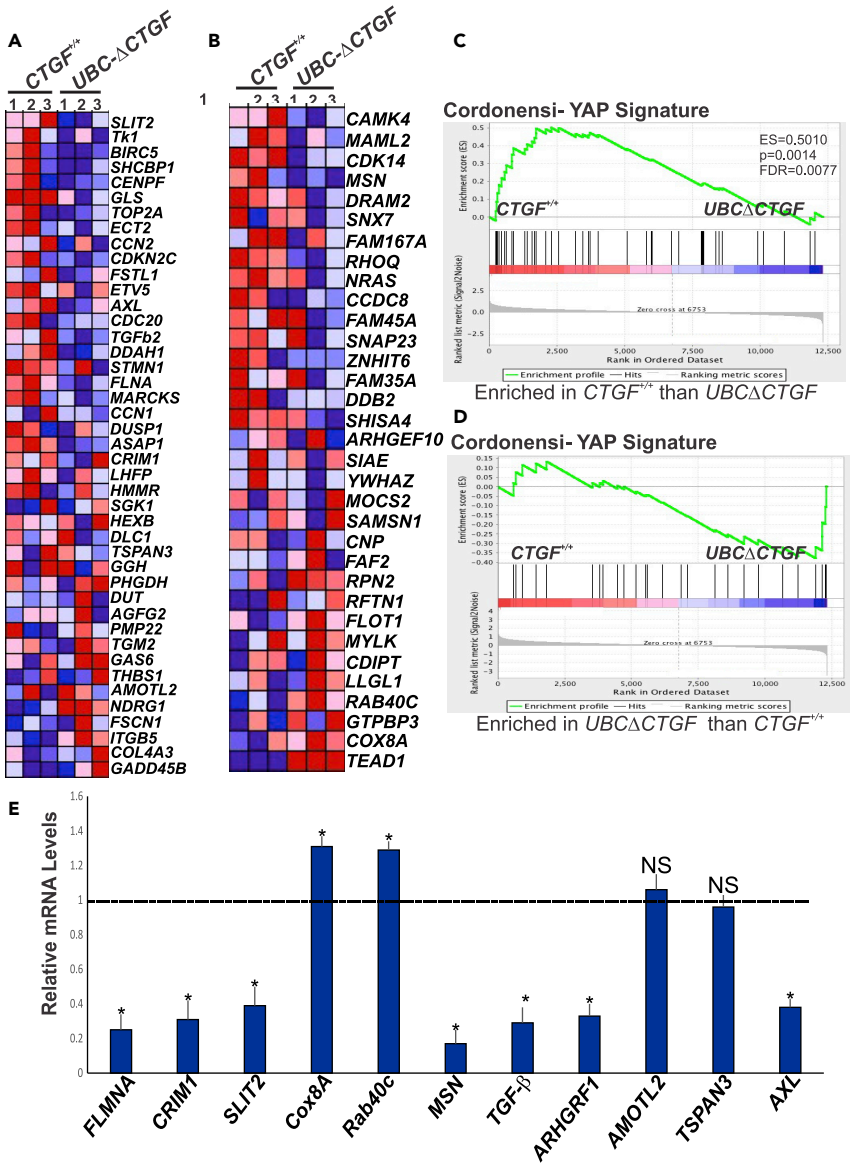

Figure 5. CTGF-Dependent Transcriptional Program Targets YAP Network Genes

(A and B) Heatmaps of the top 32–43 enriched genes identified by GSEA showing differential regulation of YAP signature genes in retinas of *UBCΔCTGF* mice. Enrichment of CTGF signature with genes up-regulated in MCF10A cells (breast cancer) over-expressing YAP gene and YAP conserved signature/Hippo pathway genes are shown in (A) and (B), respectively.

(C and D) Running enrichment score for the gene set analyses shown in (A) and (B) as the analysis walks along the ranked list.

(E) Relative mRNA levels of YAP target genes in retinal lysates of $CTGF^{+/+}$ and *UBCΔCTGF* mice. The mRNA levels in $CTGF^{+/+}$ mice were set to 1. Each measurement was performed in triplicate. (*$p < 0.05$, $n = 3$).

YAP in the underlying mechanisms of *CTGF*-dependent regulation of angiogenesis, we determined whether the transcriptomic changes associated with *CTGF* deficiency correlated with those caused by YAP deletion (or overexpression). Using GSEA and previously reported data for YAP overexpression in the Msig (Liberzon et al., 2015), we found that numerous genes that were upregulated upon YAP stimulation were decreased by *CTGF* deletion (e.g., Filamin A, ASAP1, CRIM1, SLIT2) (Figures 5A–5D). Reversibly, genes that were downregulated upon YAP stimulation were upregulated upon *CTGF* deletion (e.g., Cox8A, RAB40C). For further *CTGF* target gene data validation, we analyzed 11 differentially expressed YAP network genes by qPCR. As shown in Figure 5E, the expression of 9 of the 11 genes was fully consistent

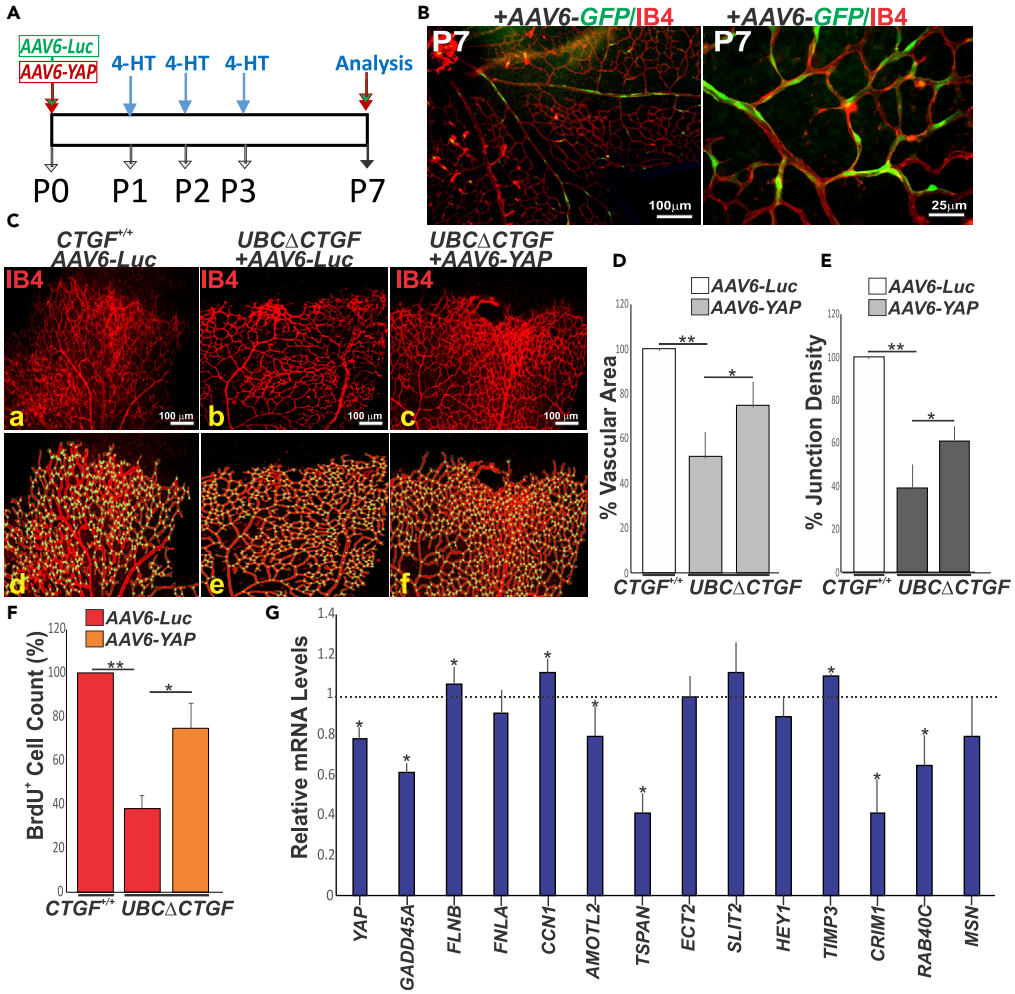

Figure 6. YAP-Mediated Rescue of Vascular Defect Caused by *CTGF* Deletion

(A) Schematic representation of *AAV6*-mediated rescue protocol of *CTGF* deletion following AAV6-mediated expression of *YAP*. The *AAV6* vector is injected at P1 followed by 4HT injection at P2, P3, and P4 to induce *CTGF* deletion. Vascular phenotype is analyzed at P7.

(B) Flat-mount images of IB4-stained retinas from $CTGF^{+/+}$ mice at P7 following retro-orbital injection of *AAV6-GFP*. Note that *GFP* expression is largely found in the retinal vascular endothelium lining blood vessels.

(C) IB4-stained retinal mounts of $CTGF^{+/+}$ (a) and *UBCΔCTGF* (b and c) mice following retro-orbital injection of either *AAV6-luc* (a and b) or AAV6-*YAP* (c). Analyses of vascular parameters (i.e., vascular area and junction density) performed with AngioTool software are shown in (d–f) as described in Figure 2A.

(D and E) Graphical representations of the changes in vascular area, junction density, and lacunarity between control and experimental groups described in Figure 6C. **p < 0.001 and *p < 0.05 versus $CTGF^{+/+}$ (n = 4).

(F) Proliferation index as determined by $BrdU^+$ nucleus counts in retinal mounts of $CTGF^{+/+}$ and *UBCΔCTGF* mice following retro-orbital injection of either *AAV6-luc* or *AAV6-YAP*. Data are means ± SE. *$p < 0.05$; **$p<0.001$.

(G) Relative mRNA levels of YAP target genes in retinal lysates from $CTGF^{+/+}$ and *UBCΔCTGF* mouse retinas. The mRNA levels in $CTGF^{+/+}$ mouse retinas were set to 1. Each measurement was performed in triplicate. (*p < 0.05, *n* = 3).

with their RNA-seq expression profiles and trends ($p < 0.05$), suggesting that the *CTGF*-dependent transcriptional program is, at least in part, linked to YAP regulatory activities. As *CTGF* is itself a YAP target gene (Zhao et al., 2008), the expression and activity of *CTGF* and YAP are mutually regulated.

YAP-Mediated Rescue of Vascular Defects Caused by *CTGF* Deficiency

To further examine the extent of YAP involvement in *CTGF*-dependent effects on vascular development, we determined whether ectopic re-expression of *YAP* could rescue the vascular defects associated with *CTGF* deletion. To this end, *YAP* was ectopically expressed through adeno-associated virus isotype 6

(AAV6)-mediated gene transfer (Figure 6A). Retro-orbital injection of a control *AAV6-GFP* vector into P1 mouse pups produced efficient expression of the *GFP* transgene in ECs lining retinal blood vessels at P7 (Figure 6B). Quantitative analyses of the retinal vascular phenotype at P7 showed that AAV-mediated re-expression of *YAP* significantly increased vascular area and junction density in *UBCΔCTGF* mice compared with those injected with the AAV6-control transgene (i.e., AAV6-Luciferase or AAV6-Luc) (Figures 6C–6E). Similarly, $BrdU^+$ cell count was significantly increased upon re-expression of YAP in *CTGF*-deficient mice, which is consistent with increased cell proliferation in sprouting vessels (Figure 6F). qPCR-based analyses of mRNA contents showed that YAP re-expression primarily affected genes involved in cell adhesion and migration (e.g., *CCN1*, *TSPAN*, *CRIM1*), proliferation (e.g., *ECT2*, *SLIT2*), differentiation (e.g., *HEY1*), and ECM remodeling (e.g., *TIMP3*) (Figure 6G). These gene targets are under direct or indirect regulation by YAP (Kim et al., 2015, 2016), suggesting that YAP acts as a relay for *CTGF*-dependent control of EC growth.

Regulation of the Paracellular Vascular Barrier through CTGF-YAP Functional Interaction

Next, we determined whether *YAP* re-expression may also improve vascular permeability defects associated with *CTGF* deletion. As shown in Figure 7A, FITC-albumin extravasation was markedly reduced in *UBCΔCTGF* mouse retinas transduced with AAV6-YAP compared with those transduced with the AAV6-Luc control. When normalized to the vascular area, re-expression of *YAP* significantly reduced vascular leakage in *CTGF* mutant mouse retinas compared with their control counterparts (Figure 7B).

A defining feature of a functional retinal barrier is (1) a low rate of receptor- and transporter-mediated endocytosis (i.e., transcellular permeability) across ECs and (2) the expression of TJ and AJ proteins that limit paracellular permeability between adjacent ECs (Park-Windhol and D'Amore, 2016) (Figure 7C). Proteins involved in transcellular (endocytic) transport include plasmalemma vesicle-associated protein (PLVAP), dynamin-1 and dynamin-2, pacsin 2, flotillin-1 and flotillin-2, Msfd2a, and the glucose transporter Glut1 (Bosma et al., 2018). Our GSEA data showed that the transcriptomic changes associated with *CTGF* deletion did not include these transcellular permeability genes (Figures 7D and 7E). The mRNA levels of *PLVAP*, one of the most important endothelial genes encoding a structural protein of fenestral and stomatal diaphragms (van der Wijk et al., 2019), were not affected by either loss of *CTGF* function or *YAP* re-expression (Figure 7F), suggesting that CTGF signals do not target genes encoding transcellular transport proteins.

Next, we examined the effects of CTGF signals on EC-EC junction proteins that regulate the paracellular barrier in the retina. Quantitative analyses by qPCR showed that the expression of *cadherin 5* (also known as *CDH5* or *VE-cadherin*), *occludin* (OCLN), and *PECAM1* was not altered in *UBCΔCTGF* compared with $CTGF^{+/+}$ retinas (Figures 7G–7I). In addition, re-expression of *YAP* in *UBCΔCTGF* mice did not influence the transcription of these junctional protein genes either, except for *Claudin 5* (*CLDN5*). *CTGF* deletion significantly reduced *CLDN5* expression, although ectopic *YAP* expression had no effect on *CLDN5* gene transcription in the retina (Figure 7J). *CLDN5* deficiency in mice was reported to affect vascular barrier to small (<0.8 kDa) molecules only (Nitta et al., 2003). As such, changes in Claudin 5 protein levels alone may not account for the vascular barrier breakdown in *CTGF*-deficient mice.

Meanwhile, even though the expression of *CDH5*, the EC-specific core regulator of vascular integrity and quiescence, was unchanged in *CTGF* mutant versus WT retinas, CDH5 phosphorylation is a major regulatory step leading to increased trans-vascular flux of fluid and proteins. CDH5 cytoplasmic phosphorylation displaces p120-catenin and β-catenin from AJs, thereby increasing endothelial permeability (Dejana et al., 2008). Immunohistochemical analysis of the pattern of CDH5 distribution showed that both WT and *CTGF* mutant retinal vessels exhibited straight CDH5-stained junctions characteristic of stable mature junction as well as endocytic CDH5 vesicles typical of CDH5 turnover and remodeling activities (Figure 7L). However, analysis of phosphorylated CDH5 did not reveal changes in CDH5 phosphorylation at Tyr 731 between WT and *CTGF* mutant retinas (Figure 7M), suggesting that CTGF regulation of the paracellular barrier may not be controlled through a CDH5 phosphorylation cascade. Importantly, because YAP is also a component of AJ and TJ complexes, it is reasonable to surmise that the remarkable reduction of YAP expression in *CTGF*-deficient mice (Figure 7K) could be responsible for the associated vascular leakage.

Reduced YAP Levels Destabilized Junctional Complexes in *CTGF*-Deficient ECs

YAP has been shown to associate with junctional protein complexes in stabilized TJs and AJs (Giampietro et al., 2015; Neto et al., 2018). To examine the role of the *CTGF*/YAP axis in the regulation of the paracellular barrier, we derived ECs from the brain tissue of *UBCΔCTGF* mice and their WT littermates and cultured

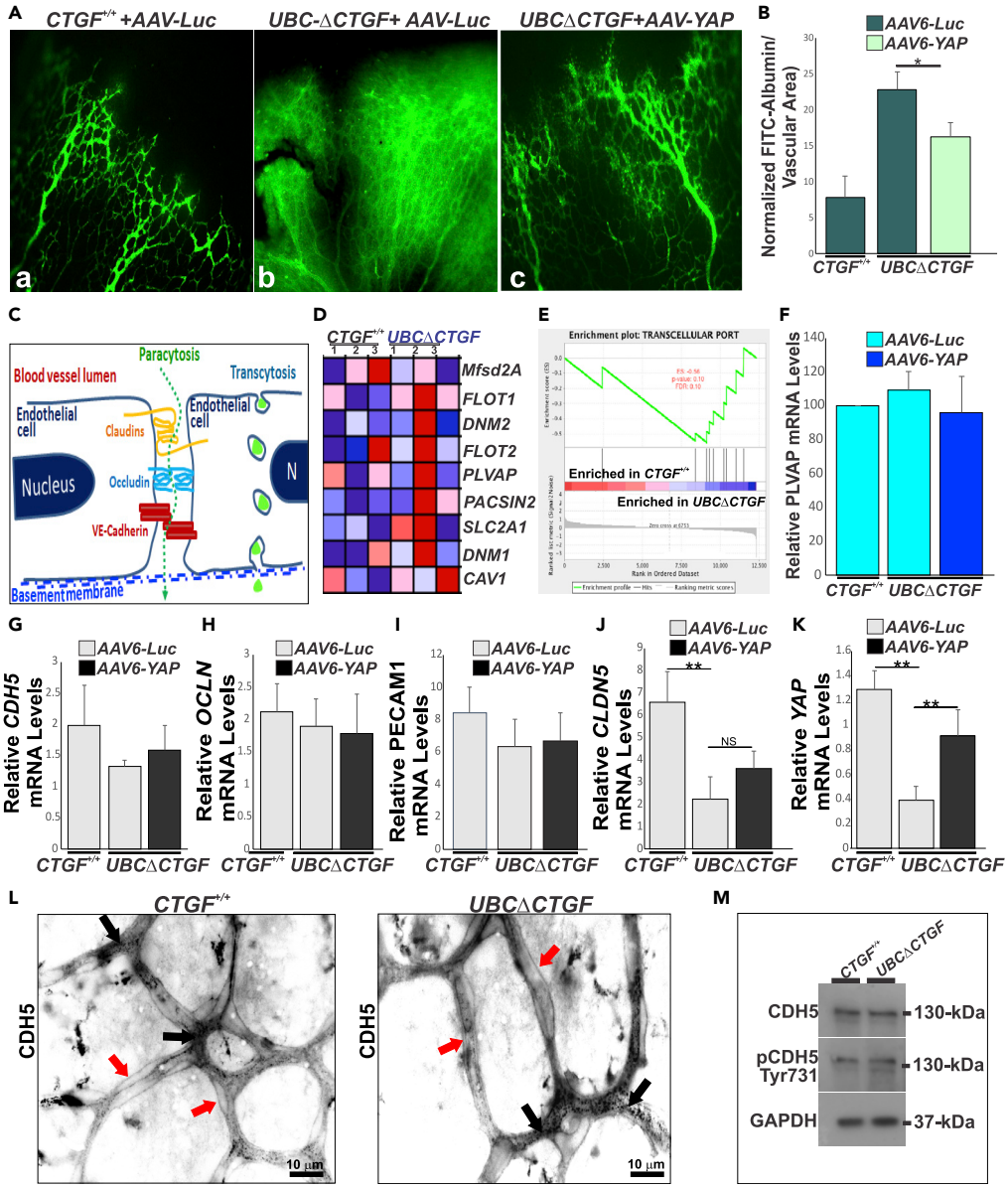

Figure 7. Regulation of the Paracellular Vascular Barrier through CTGF-YAP Functional Interaction

(A and B) (A) Retinal flat mounts of *CTGF*$^{+/+}$ (a) and *UBCΔCTGF* (b and c) mice following retro-orbital injection of FITC-albumin. *CTGF*$^{+/+}$ and *UBCΔCTGF* mice were transduced with either *AAV6-luc* (a and b) or *AAV6-YAP* (c). AAV vector injection and 4HT-induced *CTGF* exon recombination were as described in Figure 6A. Vascular permeability index in these groups is shown in (B). *p<0.05.

(C) Diagram outlining paracellular and transcellular transports in the endothelium.

(D and E) (D) GSEA-generated heatmap of CTGF transcriptome enrichment with transcellular transport proteins. Range of colors (red to blue) indicates the range of expression values (high to low). The enrichment score (ES) plot for transcellular gene set is shown in (E).

(F–K) Relative mRNA levels of transcellular (e.g., (F) *PLVAP*) and paracellular (e.g., (G) *CDH5*, (H) *OCLN*, (I) *PECAM1*, (J) *CLDN5*, and (K) *YAP*) in retinal lysates of *CTGF*$^{+/+}$ and *UBCΔCTGF* mice. Each experimental point was performed in triplicate. (**p < 0.05, *n* = 3).

(L) High-magnification images of retinal vessels of P7 *CTGF*$^{+/+}$ and *UBCΔCTGF* mice stained with CDH5 antibodies. Single-channel images of retinal capillaries are shown. Straight mature CDH junctions are shown with red arrows. Vesicular endocytic CDH5 vesicles are shown with black arrows.

(M) A representative image of western blot analysis of CDH5 and pCDH5 (Tyr 731) in retinal lysates from WT and *UBC*ΔCTGF mice. GAPDH was used as a loading control.

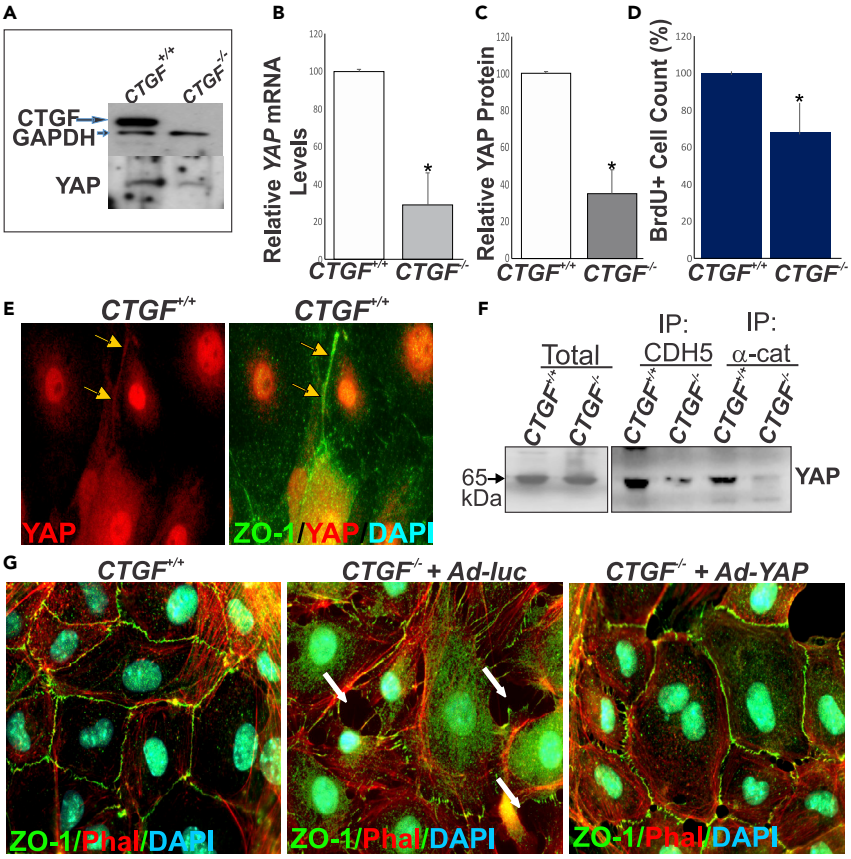

Figure 8. Reduced YAP Levels Destabilized Junctional Complexes in *CTGF*-Deficient ECs

(A) Expression of CTGF and YAP proteins in ECs explanted from $CTGF^{+/+}$ and *UBC*Δ*CTGF* (i.e., $CTGF^{-/-}$) mouse brain as determined by western blotting. GAPDH was used as a loading control.

(B and C) Relative *YAP* (B) mRNA and (C) protein levels in EC lysates of $CTGF^{+/+}$ and $CTGF^{-/-}$ mice. *$p < 0.05$ ($n = 3$).

(D) Proliferation index of ECs cultured from $CTGF^{+/+}$ and $CTGF^{-/-}$ mice as determined by cell count. *$p < 0.05$ ($n = 3$).

(E) Immunohistochemical localization of YAP in ECs explanted from $CTGF^{+/+}$ mouse brain mice. Colocalization with ZO-1 is shown.

(F) Immunoprecipitation of cultured EC protein extracts from $CTGF^{+/+}$ and $CTGF^{-/-}$ mice. Protein extracts were immunoprecipitated with anti-CDH5 and anti-α-catenin, and further immunodetection was performed with antibodies against YAP.

(G) Immunohistochemical staining with phalloidin and ZO-1 antibody of $CTGF^{+/+}$ and $CTGF^{-/-}$ mouse ECs grown to confluence. Arrows indicate location of intercellular gaps at EC-EC junctions. A representative image of adenovirus-mediated re-expression of *YAP* is shown.

them to confluence for subsequent *in vitro* experiments. Under normal culture conditions, *CTGF*-deficient ECs showed reduced levels of YAP at the mRNA and protein levels (Figures 8A–8C). $BrdU^{+}$ cell count was significantly reduced in *CTGF*-deficient ECs, which is consistent with the role of CTGF and YAP in promoting EC proliferation (Figure 8D). In $CTGF^{+/+}$-derived cells, YAP localized to the cytoplasm, nucleus, and cell-cell junctions (Figure 8E). Co-immunoprecipitation and western blot analyses revealed that YAP forms a complex containing CDH5/VE-cadherin and α-catenin, corroborating the association of YAP with junctional proteins (Figure 8F). However, the levels of YAP-containing protein complexes were markedly reduced in $CTGF^{-/-}$-derived cells. Furthermore, phalloidin-labeled, ZO1-stained cells showed that *CTGF* mutant ECs exhibited numerous intercellular gaps wherein cell borders (delineated by ZO1 staining) change from straight to zigzag lines (Figure 8G), which is indicative of and consistent with disrupted cell-cell junctions. Adenovirus-mediated re-expression of *YAP*, at least in part, reduced intercellular gaps and re-established continuous cell-cell demarcation lines. Together, these observations suggest that CTGF-induced *YAP* expression is, at least in part, critical for both EC growth and formation and maintenance of stable junctional complexes at cell-cell contacts.

DISCUSSION

The matricellular protein CTGF is known to achieve numerous cell type-specific functions in the immediate microenvironment of the cells. CTGF signals regulate cell proliferation, differentiation, adhesion, migration, and epithelial-mesenchymal transition (Krupska et al., 2015; Leask, 2019). These effects are mediated by a CTGF interactome that includes integrin and non-integrin receptors, other cell surface molecules (e.g., HSPGs, LRPs), ECM, and growth factors (Lau, 2016). CTGF-integrin interactions induced angiogenesis in rat cornea (Babic et al., 1999) and in chick chorioallantoic membranes (Shimo et al., 1999). However, CTGF was also shown to inhibit angiogenesis *in vitro* by physically interacting with and sequestering VEGF in an inactive form (Inoki et al., 2002). Although these *in vitro* and *ex vivo* studies provided insightful information about the molecular properties of the CTGF protein, they did not integrate exogenous cues such as exposure to heterogeneous cell-cell interactions, flow and associated shear stress effects, and tissue-derived signals.

Using transgenic mouse models, targeted gene disruption, and "omic" approaches, we showed that CTGF provides a unique microenvironment in the vascular wall that fine-tunes angiogenesis and ensures barrier integrity. First, we showed that *CTGF* was robustly expressed primarily in endothelial stalk cells and secondarily in pericytes and glia during postnatal retinal vascular development and its expression persisted in the adult vasculature. In ECs, the expression was limited to cells making new cell-cell contacts, whereas ECs prone to occupy the tip cell position were CTGF-negative. These observations are in congruence with previous reports describing widespread expression of *CTGF* mRNA in the embryonic vascular system and constitutive regulation of the *CTGF* gene in ECs (Friedrichsen et al., 2003; Ivkovic et al., 2003). Hemodynamic forces, which play a critical role in determining the synthetic phenotype and function of ECs, are major inducers of *CTGF* gene expression (Chaqour and Goppelt-Struebe, 2006; Yoshisue et al., 2002). Indeed, tip cells at the sprouting vascular front experience very low levels of shear (Bernabeu et al., 2014) and minimally express, if at all, CTGF, suggesting that blood flow-induced shear deformation, which increases EC capacity to orient in the direction of the flow in newly lumenized vessels, is a potentially important inducer of *CTGF* gene expression in the endothelium. Interestingly, a study by Friedrichsen et al. revealed a dichotomized *CTGF* expression pattern in mouse embryos with higher *CTGF* mRNA levels in the pressured arteries (e.g., aorta, pulmonary, and peripheral arteries) than low-pressured veins (e.g., vena cava) (Friedrichsen et al., 2003). Congruently, our findings in the CTGF promoter reporter mouse retina showed that the *CTGF*:*GFP* reporter was expressed in ECs of the arterial and capillary walls, whereas venous ECs minimally expressed the CTGF:GFP reporter. Thus, the underlying basis for differential expression of *CTGF* between arterial and venous ECs is conceptually valid and strong. However, differential *CTGF* mRNA levels between ECs cultured from arterial (e.g., coronary arteries) and venous (e.g., HUVECS) vessels could not be detected when these cells were cultured under static conditions (data not shown), suggesting that differential pressure signals between arteries and veins could account for variations of CTGF gene regulation in arterial and venous ECs. However, it is noteworthy that the *CTGF*:*GFP* reporter was expressed in mural ensheathing cells of arteries, capillaries, and veins. This observation is at variance with Friedrichsen et al.'s study, which did not show *CTGF* mRNA signals in venous mural cells such as those of the vena cava. Such discrepancy between those findings and ours may be attributed to the methodology used to detect *CTGF* mRNA and protein signals, or it could be attributed to differences between the vascular bed types analyzed, blood vessel diameter/caliber, and/or three-dimensional geometry of the vessels. In addition, the confounding effects of transcriptional and post-transcriptional regulatory mechanisms of the *CTGF* gene could also account for differences in mRNA and protein signals.

Our data further demonstrated that global or EC-specific deletion of *CTGF* altered normal retinal vascular development. Loss of CTGF function at postnatal stages caused hypovascularization of the retina and altered vascular permeability, recapitulating the vascular defects characteristic of early-onset familial exudative vitreoretinopathy in humans (Kramer et al., 2016). *CTGF* deficiency reduced vascular area, density, and junctional point numbers, and increased vascular lacunarity, which was correlated with a significant decrease of EC proliferation. However, *CTGF* deficiency did not alter tip cell number and hierarchical specification of the vasculature into arteries, capillaries, and veins, indicating that *CTGF* expression does not affect the dynamics of EC phenotypical plasticity. Interestingly, global or EC-specific deletion of *CTGF* produced vascular defects similar to those associated with deletion of transcription factors such as *SRF* and *MRTF-A* (Weinl et al., 2015), two versatile transcription factors that toggle between disparate programs of gene expression related to cell growth and differentiation (Sun et al., 2006). Indeed, the *CTGF* gene is one of the CArG-box-containing promoter genes (i.e., CarGome) that is activated by the SRF/MRTF

duo. Thus, CTGF can potentially act as an SRF/MRTF downstream effector molecule, mediating their regulatory effects on EC growth and function.

A previous study by Hall-Glenn et al. showed that a global *CTGF* deficiency in mice induced minor enlargement of blood vessels and local edema in the *CTGF* mutant dermis (Hall-Glenn et al., 2012). These changes have been attributed to incomplete coverage of microvessels by pericytes in the dermis of *CTGF* mutant mice. However, it was unclear whether the observed vascular phenotype was due to direct effects in ECs or secondary CTGF effects in other cell types. Our data showed that the angiogenic defects associated with CTGF deletion were largely due to the loss of EC-derived CTGF as EC-specific deletion of *CTGF* recapitulated, at least in part, those of its ubiquitous deletion. Because loss of *CTGF* function reduced EC proliferation, and sprouting, it appears to potentiate the effects of other regulators of angiogenesis. It is noteworthy that the loss of pericyte-derived CTGF minimally, if at all, altered vascular growth and integrity. The importance of pericytes in the development and function of microvessels has been well established, as illustrated by the phenotype of mice in which pericyte development has been disrupted (Enge et al., 2002). Therefore, targeting an important component of their secretome would be expected to have a greater impact during angiogenesis. More than one explanation is possible to rationalize the lack of retinal vascular defects in mice with pericyte-specific *CTGF* deletion. First, pericyte-specific knockdown of CTGF was not fully penetrant due to the expression of CTGF by cells other than $NG2^+$ cells. Under these circumstances, the role of CTGF produced by ECs and glia may be magnified, fully compensating for the absence of pericyte-derived CTGF. Second, pericyte-specific deletion of *CTGF* was produced using transgenic mice expressing the Cre recombinase under the control of the *NG2* (aka *Cspg4*) promoter/enhancer. As *NG2* expression is restricted to arteriolar and capillary perivascular cells during angiogenesis (Chan-Ling and Hughes, 2005), Cre-mediated *CTGF* gene targeting with the *NG2* promoter may be limited to $NG2^+$ cell subpopulation of pericytes only, and this was inconsequential on the vascular phenotype. Third, the retinal model of angiogenesis that was used in our experiments is based on postnatal angiogenesis, even though the bulk of developmental angiogenesis occurs during embryonic stages. Therefore, it was not surprising that constitutive deletion of *CTGF* was reported to cause incomplete coverage of microvessels by pericytes in the dermis of *CTGF* mutant embryos (Hall-Glenn et al., 2012). This suggests that *CTGF* deficiency in pericytes may have a lesser impact during the postnatal than embryonic stages. Last, the effects of pericyte-derived CTGF may be minimal during normal postnatal angiogenic events but more effective in pathological events. Future studies addressing this hypothesis are warranted.

Molecularly, several clusters of genes and pathways involved in the regulation of important processes such as EC proliferation, migration, and junction formation were affected by *CTGF* deficiency. The expression of *IGF-1*, *TGF-β1*, *TGF-β2*, *FGF-10*, and *angiopoietin 1* was downregulated upon *CTGF* deletion, and reduced expression of these growth factor genes may account for the subsequent hypovascularization of the retina. Similarly, loss of *CTGF* function decreased the expression of several key basement membrane (BM) protein genes such as *laminin 4*, *collagen 4A1*, *SPARC*, and *tenascin C* as well as other FACIT collagens and proteoglycans, many of which are important for the stability and compliance properties of the vascular wall.

In addition, several transcription factors and co-cofactors showed differential gene expression patterns between WT and mutant *CTGF* mouse retinas including *YAP*, *NFAT5*, and *SRF*. *CTGF* deletion significantly decreased the expression of these transcriptional regulators, many of which affect important aspects of vascular cell growth and differentiation. *YAP* regulation by CTGF signals is of particular significance as, thus far, *YAP* has been shown to be regulated largely at the post-translational levels by G-protein-coupled receptors (GPCR), mechanical forces, growth factors such as VEGF, actin dynamics, and Lats1 activity (Aragona et al., 2013; Avruch et al., 2012). The regulation of *YAP* expression by CTGF is highly significant in developmental angiogenesis, although the transcriptional or post-transcriptional mechanisms underlying such regulation remain to be determined. The autonomous role of YAP on vessel development has previously been reported in several independent studies using EC-specific deletion of *YAP* and *TAZ*, a paralog of *YAP* that also regulates gene expression through binding to YAP-interacting partners (Hong and Guan, 2012). Double knockout of *YAP* and *TAZ* in the endothelium decreased vascular density, branching, and sprouting (Choi et al., 2015), mimicking, at least in part, the *CTGF* loss-of-function phenotype. Concordantly, we found a significant gene profile overlap of CTGF and YAP target genes. It is conceivable that *YAP* expression and activity in ECs build a transcriptional response that sustains CTGF signals by coordinating the expression of sets of genes and proteins that regulate various aspects of sprouting angiogenesis.

YAP is a critical control node in cell fate decisions of proliferation, differentiation, survival, or apoptosis. Nuclear YAP physically interacts with DNA-binding transcription factors such as RUNX family, thyroid TF1 (TTF-1), TBX5, PAX3, PAX8, peroxisome proliferator-activated receptor γ, and TEAD to stimulate or repress the expression of downstream target genes (Panciera et al., 2017). The TEAD family of transcription factors plays an important role in YAP-dependent gene regulation and cell growth stimulation. The TEAD consensus sequences were found in at least 75% YAP target genes, as YAP and TEAD1 co-occupied >80% of the promoters pulled down by chromatin immunoprecipitation (Zanconato et al., 2015). Surprisingly, our data showed that whereas *YAP* gene expression was downregulated upon *CTGF* deletion, the expression of *TEAD1* was upregulated in the *CTGF*-deficient mouse retina. These findings raise the question whether YAP and TEAD act independently of one another to control separate angiogenic programs. Recent studies provided an answer to this question. By investigating the biology of GPCR-activated YAP/TAZ during retinal angiogenesis, Yasuda et al. have shown that YAP acts independently of TEAD to suppress the expression of Dll4, a transmembrane ligand for the Notch family of receptors, which prevents overexuberant angiogenic sprouting (Yasuda et al., 2019). This suggests an essential role of TEAD-independent YAP activities in retinal angiogenesis. This is also consistent with other findings by Zhao et al. showing that TEAD binding-defective YAP-S94A mutant can still induce expression of a fraction of the YAP-regulated genes (Zhao et al., 2008). Further studies will be needed to tease apart the full spectrum of YAP-independent TEAD and TEAD-independent YAP functions in angiogenesis and determine whether increased TEAD1 expression in CTGF-deficient mice preserves/bolsters YAP-independent TEAD1 angiomodulatory activities. Importantly, CTGF and YAP are both molecular effectors and downstream targets of mechanical forces, as their expression and activity have been associated with cells exposed to mechanical stresses, such as shear stress, stretching, or stiffness of the surrounding ECM (Bertero et al., 2016; Dupont et al., 2011; Wang et al., 2016). A study by Nakajima et al. in zebrafish demonstrated that endothelial YAP functions in response to flow to maintain EC function in blood vessels (Nakajima and Mochizuki, 2017). The flow-induced reorganization of F-actin was associated with the release of YAP from angiomotin and its nuclear translocation during vessel growth. Molecularly, CTGF signals and YAP activity seem to reinforce the cell cytoskeleton and contractile apparatus, and through these mechanisms, they respond to and control the actomyosin-generated internal forces in the cells (Neto et al., 2018). Thus, both hemodynamic and internally generated forces in ECs potentially fuel and sustain a CTGF/YAP feedforward loop that sustains angiogenesis during vascular development.

Another important outcome of our study design is that CTGF is an important determinant of blood vessel integrity and stability. Barriergenesis in the developing retina involves the coordinated induction of proteins that maintain TJs and AJs and nutrient transporters across ECs (Obermeier et al., 2013). Thereafter, maturation of the barrier properties is achieved as functional and physical interactions occur with pericytes, astrocytes, and Müller cells. Assembly and maturation of junctional complexes between ECs are dependent on actomyosin dynamics regulated by the activity of small Rho GTPases such as RhoA and Cdc42 (Aoyama et al., 2012), which appears to be required for maintenance of blood barrier integrity during adulthood as well. However, the acquisition of endothelial barrier properties in *CTGF*-deficient retinas was not due to defects in transcellular transport because mutant *CTGF* mice showed no differences in the expression of *PLVAP* and other membrane proteins that localize to fenestrae and caveolar stomatal diaphragms of ECs. Instead, paracellular barrier protein association and organization seemed to have been altered in *CTGF*-deficient blood vessels. *CTGF* deletion similarly altered the barrier properties of preformed vessels in adult mice suggesting that basal expression of CTGF is critical for not only barrier formation but also its maintenance. It is noteworthy that vascular leakage was not associated with active hemorrhage sites in the retina and brain in *CTGF*-deficient mice. Similarly, the initial characterization of mice with constitutive deletion of CTGF did not report visible signs of hemorrhage during embryonic and fetal development (Ivkovic et al., 2003), even though defects in ECM formation or loss of genes crucial for EC-EC and EC-ECM interaction generally led to severe hemorrhagic phenotypes (Timmer et al., 2005). However, CTGF is different from common ECM proteins because, as a matricellular protein, CTGF does not subserve a structural role in the cell environment, but functions as an extracellular cue that optimizes the function of growth factors and ECM proteins. The absence of severe hemorrhage in *CTGF* mutant mice also raises the possibility of potential functional compensation for *CTGF* deficiency by CCN1, a closely related homolog of CTGF. Both genes are highly expressed in the vascular system and have similar activities *in vitro* (Chaqour, 2013; Lee et al., 2019). Although CTGF and CCN1 orchestrate complementary aspects of developmental angiogenesis, they may also serve redundant functions in vascular elements (Chintala et al., 2015). Studies designed to contrast the vascular phenotypes of *CTGF*, *CCN1*, and *CTGF/CCN1* double mutants will be informative in this regard.

Last, our data showed that CTGF effects on the vascular permeability were, at least in part, dependent on *YAP* expression. Based on *CTGF* loss- and subsequent *YAP* gain-of-function phenotypes, reduced YAP levels in ECs disrupted intercellular junctional complex formation and stabilization. Our coimmunoprecipitation experiments showed that the presence of YAP in protein complexes of CDH5 and α-catenin is in agreement with previous findings that YAP associates with the VE-cadherin complex via 14-3-3 proteins, a family of phosphoserine-binding proteins that prevent YAP shuttling between the cytoplasm and nucleus (Giampietro et al., 2015). Hyperphosphorylated YAP localizes to adherent junctions in a trimeric complex with 14-3-3 and α-catenin indicating that YAP functions in the cytoplasm, in the nucleus, and at cell-cell junctions. We suggest that the "decision" of the endothelium to become permeable instead of forming a blood-retinal barrier is primarily dependent on YAP levels in different cell compartments. It is anticipated that conditions that perturb the functional interactions between CTGF and YAP likewise alter YAP cellular localization and vascular permeability.

Taken together, our data showed a crucial role for CTGF in regulating the expression and function of a wide array of extracellular and intracellular factors that are essential for normal vascularization of the retina and the acquisition of a functional vascular barrier. It is conceivable that genes affected by CTGF in the endothelium might be relevant for angiogenesis and barriergenesis in organs other than the retina as well. It also is highly likely that the deregulation of the CTGF network genes is relevant in pathological angiogenesis processes (e.g., diabetic retinopathy, retinopathy of prematurity) characterized by disrupted growth, lack of vessel maturation, defective remodeling, and/or barrier dysfunction. Future studies focused on the regulation and function of the CTGF/YAP angiomodulatory pathway in *in vivo* models of vascular diseases are warranted.

Limitations of the Study

The transcriptomic differences between WT and mutant CTGF mouse retinas together with previously reported vascular defects associated with loss of function of CTGF targets provided greater insights into the essential role of CTGF in retinal angiogenesis and barriergenesis. Equally important, however, is information about the retinal microvascular ultrastructure in CTGF mutant mouse retina, which is a limitation of this study. Transmission electron or two-photon microscopy is the method of choice to be used in future studies to observe and further examine retinal vessel micromorphology and assess potential loss of EC contiguity, as well as the ultrastructural changes of endothelial TJs. Nevertheless, there are prior ultrastructural analyses showing that dermal capillaries of *CTGF*-deficient mouse embryos had multiple protrusions as well as ultrastructural defects in microvascular endothelial BM protein assembly (Hall-Glenn et al., 2012). These observations are consistent with our data showing that *CTGF* deletion reduced the expression of numerous BM proteins (e.g., *laminin 4, elastin, fibrillin-2, glypican 5, collagen 4A1, and tenascin-C*). In particular, defective expression and deposition of type IV collagen and laminin 4 in *CTGF*-deficient mice could at least in part, engender ultrastructural disorganization/discontinuity of the capillary BM and breakdown of the vascular barrier as seen in acute and chronic neuropathological settings (Lau et al., 2013). As previously shown by Poschl et al., deletion of *type IV collagen* α_1 or α_2 *subunit* gene did not prevent BM formation and assembly, but reduced its stability (Poschl et al., 2004), indicating that type IV collagen is critical for the integrity of the microvasculature wall. Similarly, mice lacking *laminin 4*, exhibited a discontinuous capillary BM and vascular leakage during the embryonic and neonatal period (Thyboll et al., 2002). Clearly, by targeting the BM protein and growth factor genes, CTGF affects the maturation and barrier function of the developing blood vessels and potentially their force-bearing capabilities during neonatal life.

Resource Availability

Lead Contact

Requests for resources and reagents should be directed to and will be fulfilled by the Lead Contact, Brahim Chaqour (bchaqour@downstate.edu).

Materials Availability

All unique/stable reagents generated in this study are available from the Lead Contact with a completed Materials Transfer Agreement and reasonable compensation by requestor for shipping and handling charges.

Data and Code Availability

RNA-seq data are available at the NCBI Gene Expression Omnibus with the series record GSE146900.

METHODS

All methods can be found in the accompanying Transparent Methods supplemental file.

SUPPLEMENTAL INFORMATION

Supplemental Information can be found online at https://doi.org/10.1016/j.isci.2020.101184.

ACKNOWLEDGMENTS

We are thankful to Dr. Stephen J. Weiss (University of Michigan) for his involvement in the project conception, data discussion and interpretation, and review of the manuscript. We appreciate the technical contribution of Genesis Lopez and Xin Chen. The help of Zaid McKie-Krisberg and Christopher Armoskus for RNA-seq data formatting and submission to GEO was appreciated. We thank all past and present lab members for their contributions to the generation and characterization of genetically modified animals and discussions during the preparation of the manuscript. This work was supported in part by grants from the National Eye Institute of the National Institutes of Health (grants EY024998 and EY022091-05A1) to B.C.

AUTHOR CONTRIBUTIONS

S.M. and S.L. generated and characterized the vascular phenotype of mice with tissue-specific deletion of CTGF. J.A.C. and S.P. performed mouse genotyping and *in vitro* studies and associated immunohistochemical analyses. A.L. generated mice with floxed CTGF exons and contributed to data discussion. J.S. performed RNA-seq data analyses and GSEA. J.A.K. contributed to transcriptomic data interpretation. B.C. designed the project and experimental approaches and wrote the paper.

DECLARATION OF INTERESTS

The authors declare no competing interests.

Received: March 23, 2020
Revised: May 18, 2020
Accepted: May 18, 2020
Published: June 26, 2020

REFERENCES

Aoyama, E., Kubota, S., and Takigawa, M. (2012). CCN2/CTGF binds to fibroblast growth factor receptor 2 and modulates its signaling. FEBS Lett. *586*, 4270–4275.

Aragona, M., Panciera, T., Manfrin, A., Giulitti, S., Michielin, F., Elvassore, N., Dupont, S., and Piccolo, S. (2013). A mechanical checkpoint controls multicellular growth through YAP/TAZ regulation by actin-processing factors. Cell *154*, 1047–1059.

Asano, D., Hokazono, M., Hirano, S., Morita, A., and Nakahara, T. (2019). Cellular mechanisms of angiogenesis in neonatal rat models of retinal neurodegeneration. Int. J. Mol. Sci. *20*, 4759–4775.

Avruch, J., Zhou, D., and Bardeesy, N. (2012). YAP oncogene overexpression supercharges colon cancer proliferation. Cell Cycle *11*, 1090–1096.

Babic, A.M., Chen, C.C., and Lau, L.F. (1999). Fisp12/mouse connective tissue growth factor mediates endothelial cell adhesion and migration through integrin alphavbeta3, promotes endothelial cell survival, and induces angiogenesis in vivo. Mol. Cell Biol. *19*, 2958–2966.

Bernabeu, M.O., Jones, M.L., Nielsen, J.H., Kruger, T., Nash, R.W., Groen, D., Schmieschek, S., Hetherington, J., Gerhardt, H., Franco, C.A., et al. (2014). Computer simulations reveal complex distribution of haemodynamic forces in a mouse retina model of angiogenesis. J. R. Soc. Interfaces *11*.

Bertero, T., Oldham, W.M., Cottrill, K.A., Pisano, S., Vanderpool, R.R., Yu, Q., Zhao, J., Tai, Y., Tang, Y., Zhang, Y.Y., et al. (2016). Vascular stiffness mechanoactivates YAP/TAZ-dependent glutaminolysis to drive pulmonary hypertension. J. Clin. Invest. *126*, 3313–3335.

Bishop, P.N. (2015). The role of extracellular matrix in retinal vascular development and preretinal neovascularization. Exp. Eye Res. *133*, 30–36.

Bosma, E.K., van Noorden, C.J.F., Schlingemann, R.O., and Klaassen, I. (2018). The role of plasmalemma vesicle-associated protein in pathological breakdown of blood-brain and blood-retinal barriers: potential novel therapeutic target for cerebral edema and diabetic macular edema. Fluids Barriers CNS *15*, 24.

Bou-Gharios, G., Ponticos, M., Rajkumar, V., and Abraham, D. (2004). Extra-cellular matrix in vascular networks. Cell Prolif *37*, 207–220.

Chan-Ling, T., and Hughes, S. (2005). NG2 can be used to identify arteries versus veins enabling the characterization of the different functional roles of arterioles and venules during microvascular network growth and remodeling. Microcirculation *12*, 539–540, author reply 540-531.

Chaqour, B. (2013). Molecular control of vascular development by the matricellular proteins (Cyr61/CCN1) and (CTGF/CCN2). Trends Dev. Biol. *7*, 59–72.

Chaqour, B., and Goppelt-Struebe, M. (2006). Mechanical regulation of the Cyr61/CCN1 and CTGF/CCN2 proteins. FEBS J. *273*, 3639–3649.

Chintala, H., Krupska, I., Yan, L., Lau, L., Grant, M., and Chaqour, B. (2015). The matricellular protein CCN1 controls retinal angiogenesis by targeting VEGF, Src homology 2 domain phosphatase-1 and Notch signaling. Development *142*, 2364–2374.

Chintala, H., Liu, H., Parmar, R., Kamalska, M., Kim, Y.J., Lovett, D., Grant, M.B., and Chaqour, B. (2012). Connective tissue growth factor regulates retinal neovascularization through p53 protein-dependent transactivation of the matrix metalloproteinase (MMP)-2 gene. J. Biol. Chem. *287*, 40570–40585.

Choi, H.J., Zhang, H., Park, H., Choi, K.S., Lee, H.W., Agrawal, V., Kim, Y.M., and Kwon, Y.G. (2015). Yes-associated protein regulates endothelial cell contact-mediated expression of angiopoietin-2. Nat. Commun. *6*, 6943.

Chow, B.W., and Gu, C. (2015). The molecular constituents of the blood-brain barrier. Trends Neurosci. *38*, 598–608.

Dean, R.A., Butler, G.S., Hamma-Kourbali, Y., Delbe, J., Brigstock, D.R., Courty, J., and Overall, C.M. (2007). Identification of candidate angiogenic inhibitors processed by matrix metalloproteinase 2 (MMP-2) in cell-based proteomic screens: disruption of vascular endothelial growth factor (VEGF)/heparin affin regulatory peptide (pleiotrophin) and VEGF/Connective tissue growth factor angiogenic inhibitory complexes by MMP-2 proteolysis. Mol. Cell Biol. *27*, 8454–8465.

Dejana, E., Orsenigo, F., and Lampugnani, M.G. (2008). The role of adherens junctions and VE-cadherin in the control of vascular permeability. J. Cell Sci. *121*, 2115–2122.

Dupont, S., Morsut, L., Aragona, M., Enzo, E., Giulitti, S., Cordenonsi, M., Zanconato, F., Le Digabel, J., Forcato, M., Bicciato, S., et al. (2011). Role of YAP/TAZ in mechanotransduction. Nature *474*, 179–183.

Enge, M., Bjarnegard, M., Gerhardt, H., Gustafsson, E., Kalen, M., Asker, N., Hammes, H.P., Shani, M., Fassler, R., and Betsholtz, C. (2002). Endothelium-specific platelet-derived growth factor-B ablation mimics diabetic retinopathy. EMBO J. *21*, 4307–4316.

Friedrichsen, S., Heuer, H., Christ, S., Winckler, M., Brauer, D., Bauer, K., and Raivich, G. (2003). CTGF expression during mouse embryonic development. Cell Tissue Res. *312*, 175–188.

Fruttiger, M. (2007). Development of the retinal vasculature. Angiogenesis *10*, 77–88.

Gao, R., and Brigstock, D.R. (2004). Connective tissue growth factor (CCN2) induces adhesion of rat activated hepatic stellate cells by binding of its C-terminal domain to integrin alpha(v)beta(3) and heparan sulfate proteoglycan. J. Biol. Chem. *279*, 8848–8855.

Giampietro, C., Disanza, A., Bravi, L., Barrios-Rodiles, M., Corada, M., Frittoli, E., Savorani, C., Lampugnani, M.G., Boggetti, B., Niessen, C., et al. (2015). The actin-binding protein EPS8 binds VE-cadherin and modulates YAP localization and signaling. J. Cell Biol. *211*, 1177–1192.

Gupta, S., Clarkson, M.R., Duggan, J., and Brady, H.R. (2000). Connective tissue growth factor: potential role in glomerulosclerosis and tubulointerstitial fibrosis. Kidney Int. *58*, 1389–1399.

Hall-Glenn, F., De Young, R.A., Huang, B.L., van Handel, B., Hofmann, J.J., Chen, T.T., Choi, A., Ong, J.R., Benya, P.D., Mikkola, H., et al. (2012). CCN2/connective tissue growth factor is essential for pericyte adhesion and endothelial basement membrane formation during angiogenesis. PLoS One *7*, e30562.

Hashimoto, G., Inoki, I., Fujii, Y., Aoki, T., Ikeda, E., and Okada, Y. (2002). Matrix metalloproteinases cleave connective tissue growth factor and reactivate angiogenic activity of vascular endothelial growth factor 165. J. Biol. Chem. *277*, 36288–36295.

Hong, W., and Guan, K.L. (2012). The YAP and TAZ transcription co-activators: key downstream effectors of the mammalian Hippo pathway. Semin. Cell Dev. Biol. *23*, 785–793.

Inoki, I., Shiomi, T., Hashimoto, G., Enomoto, H., Nakamura, H., Makino, K., Ikeda, E., Takata, S., Kobayashi, K., and Okada, Y. (2002). Connective tissue growth factor binds vascular endothelial growth factor (VEGF) and inhibits VEGF-induced angiogenesis. FASEB J. *16*, 219–221.

Ivkovic, S., Yoon, B.S., Popoff, S.N., Safadi, F.F., Libuda, D.E., Stephenson, R.C., Daluiski, A., and Lyons, K.M. (2003). Connective tissue growth factor coordinates chondrogenesis and angiogenesis during skeletal development. Development *130*, 2779–2791.

Kim, J., Kim, Y.H., Kim, J., Park, D.Y., Bae, H., Lee, D.H., Kim, K.H., Hong, S.P., Jang, S.P., Kubota, Y., et al. (2017). YAP/TAZ regulates sprouting angiogenesis and vascular barrier maturation. J. Clin. Invest. *127*, 3441–3461.

Kim, J.Y., Park, R., Lee, J.H., Shin, J., Nickas, J., Kim, S., and Cho, S.H. (2016). Yap is essential for retinal progenitor cell cycle progression and RPE cell fate acquisition in the developing mouse eye. Dev. Biol. *419*, 336–347.

Kim, M., Kim, T., Johnson, R.L., and Lim, D.S. (2015). Transcriptional co-repressor function of the hippo pathway transducers YAP and TAZ. Cell Rep. *11*, 270–282.

Kireeva, M.L., Latinkic, B.V., Kolesnikova, T.V., Chen, C.C., Yang, G.P., Abler, A.S., and Lau, L.F. (1997). Cyr61 and Fisp12 are both ECM-associated signaling molecules: activities, metabolism, and localization during development. Exp. Cell Res. *233*, 63–77.

Kramer, G.D., Say, E.A., and Shields, C.L. (2016). Simultaneous novel mutations of LRP5 and TSPAN12 in a case of familial exudative vitreoretinopathy. J. Pediatr. Ophthalmol. Strabismus *53*, e1–5.

Krupska, I., Bruford, E.A., and Chaqour, B. (2015). Eyeing the Cyr61/CTGF/NOV (CCN) group of genes in development and diseases: highlights of their structural likenesses and functional dissimilarities. Hum. Genomics *9*, 24.

Lau, L.F. (2016). Cell surface receptors for CCN proteins. J. Cell Commun. Signal. *10*, 121–127.

Lau, L.W., Cua, R., Keough, M.B., Haylock-Jacobs, S., and Yong, V.W. (2013). Pathophysiology of the brain extracellular matrix: a new target for remyelination. Nat. Rev. Neurosci. *14*, 722–729.

Leask, A. (2019). A centralized communication network: recent insights into the role of the cancer associated fibroblast in the development of drug resistance in tumors. Semin. Cell Dev. Biol. https://doi.org/10.1016/j.semcdb.2019.10.016.

Leask, A., Holmes, A., and Abraham, D.J. (2002). Connective tissue growth factor: a new and important player in the pathogenesis of fibrosis. Curr. Rheumatol. Rep. *4*, 136–142.

Lee, S., Ahad, A., Luu, M., Moon, S., Caesar, J., Cardoso, W.V., Grant, M.B., and Chaqour, B. (2019). CCN1-Yes-Associated protein feedback loop regulates physiological and pathological angiogenesis. Mol. Cell Biol. *39*, https://doi.org/10.1128/MCB.00107-19.

Lee, S., Elaskandrany, M., Ahad, A., and Chaqour, B. (2017). Analysis of CCN protein expression and activities in vasoproliferative retinopathies. Methods Mol. Biol. *1489*, 543–556.

Liberzon, A., Birger, C., Thorvaldsdottir, H., Ghandi, M., Mesirov, J.P., and Tamayo, P. (2015). The Molecular Signatures Database (MSigDB) hallmark gene set collection. Cell Syst. *1*, 417–425.

Liu, S., Shi-wen, X., Abraham, D.J., and Leask, A. (2011). CCN2 is required for bleomycin-induced skin fibrosis in mice. Arthritis Rheum. *63*, 239–246.

Nakajima, H., and Mochizuki, N. (2017). Flow pattern-dependent endothelial cell responses through transcriptional regulation. Cell Cycle *16*, 1893–1901.

Nakamura-Ishizu, A., Kurihara, T., Okuno, Y., Ozawa, Y., Kishi, K., Goda, N., Tsubota, K., Okano, H., Suda, T., and Kubota, Y. (2012). The formation of an angiogenic astrocyte template is regulated by the neuroretina in a HIF-1-dependent manner. Dev. Biol. *363*, 106–114.

Neto, F., Klaus-Bergmann, A., Ong, Y.T., Alt, S., Vion, A.C., Szymborska, A., Carvalho, J.R., Hollfinger, I., Bartels-Klein, E., Franco, C.A., et al. (2018). YAP and TAZ regulate adherens junction dynamics and endothelial cell distribution during vascular development. Elife *7*, https://doi.org/10.7554/eLife.31037.

Nguyen, T.Q., Roestenberg, P., van Nieuwenhoven, F.A., Bovenschen, N., Li, Z., Xu, L., Oliver, N., Aten, J., Joles, J.A., Vial, C., et al. (2008). CTGF inhibits BMP-7 signaling in diabetic nephropathy. J. Am. Soc. Nephrol. *19*, 2098–2107.

Nitta, T., Hata, M., Gotoh, S., Seo, Y., Sasaki, H., Hashimoto, N., Furuse, M., and Tsukita, S. (2003). Size-selective loosening of the blood-brain barrier in claudin-5-deficient mice. J. Cell Biol. *161*, 653–660.

Obermeier, B., Daneman, R., and Ransohoff, R.M. (2013). Development, maintenance and disruption of the blood-brain barrier. Nat. Med. *19*, 1584–1596.

Panciera, T., Azzolin, L., Cordenonsi, M., and Piccolo, S. (2017). Mechanobiology of YAP and TAZ in physiology and disease. Nat. Rev. Mol. Cell Biol. *18*, 758–770.

Park-Windhol, C., and D'Amore, P.A. (2016). Disorders of vascular permeability. Annu. Rev. Pathol. *11*, 251–281.

Perbal, B., Tweedie, S., and Bruford, E. (2018). The official unified nomenclature adopted by the HGNC calls for the use of the acronyms, CCN1-6, and discontinuation in the use of CYR61, CTGF, NOV and WISP 1-3 respectively. J. Cell Commun. Signal. *12*, 625–629.

Pi, L., Xia, H., Liu, J., Shenoy, A.K., Hauswirth, W.W., and Scott, E.W. (2011). Role of connective tissue growth factor in the retinal vasculature

during development and ischemia. Invest. Ophthalmol. Vis. Sci. *52*, 8701–8710.

Poschl, E., Schlotzer-Schrehardt, U., Brachvogel, B., Saito, K., Ninomiya, Y., and Mayer, U. (2004). Collagen IV is essential for basement membrane stability but dispensable for initiation of its assembly during early development. Development *131*, 1619–1628.

Praidou, A., Androudi, S., Brazitikos, P., Karakiulakis, G., Papakonstantinou, E., and Dimitrakos, S. (2010). Angiogenic growth factors and their inhibitors in diabetic retinopathy. Curr. Diabetes Rev. *6*, 304–312.

Ryseck, R.P., Macdonald-Bravo, H., Mattei, M.G., and Bravo, R. (1991). Structure, mapping, and expression of fisp-12, a growth factor-inducible gene encoding a secreted cysteine-rich protein. Cell Growth Differ *2*, 225–233.

Scott, A., Powner, M.B., Gandhi, P., Clarkin, C., Gutmann, D.H., Johnson, R.S., Ferrara, N., and Fruttiger, M. (2010). Astrocyte-derived vascular endothelial growth factor stabilizes vessels in the developing retinal vasculature. PLoS One *5*, e11863.

Segarra, M., Aburto, M.R., Cop, F., Llao-Cid, C., Hartl, R., Damm, M., Bethani, I., Parrilla, M., Husainie, D., Schanzer, A., et al. (2018). Endothelial Dab1 signaling orchestrates neuro-glia-vessel communication in the central nervous system. Science *361*.

Shimo, T., Nakanishi, T., Nishida, T., Asano, M., Kanyama, M., Kuboki, T., Tamatani, T., Tezuka, K., Takemura, M., Matsumura, T., et al. (1999). Connective tissue growth factor induces the proliferation, migration, and tube formation of vascular endothelial cells in vitro, and angiogenesis in vivo. J. Biochem. *126*, 137–145.

Subramanian, A., Tamayo, P., Mootha, V.K., Mukherjee, S., Ebert, B.L., Gillette, M.A., Paulovich, A., Pomeroy, S.L., Golub, T.R., Lander, E.S., et al. (2005). Gene set enrichment analysis: a knowledge-based approach for interpreting genome-wide expression profiles. Proc. Natl. Acad. Sci. U S A *102*, 15545–15550.

Sun, Q., Chen, G., Streb, J.W., Long, X., Yang, Y., Stoeckert, C.J., Jr., and Miano, J.M. (2006). Defining the mammalian CArGome. Genome Res. *16*, 197–207.

Suzuma, K., Naruse, K., Suzuma, I., Takahara, N., Ueki, K., Aiello, L.P., and King, G.L. (2000). Vascular endothelial growth factor induces expression of connective tissue growth factor via KDR, Flt1, and phosphatidylinositol 3-kinase-akt-dependent pathways in retinal vascular cells. J. Biol. Chem. *275*, 40725–40731.

Tang, X., Muhammad, H., McLean, C., Miotla-Zarebska, J., Fleming, J., Didangelos, A., Onnerfjord, P., Leask, A., Saklatvala, J., and Vincent, T.L. (2018). Connective tissue growth factor contributes to joint homeostasis and osteoarthritis severity by controlling the matrix sequestration and activation of latent TGFbeta. Ann. Rheum. Dis. *77*, 1372–1380.

Thyboll, J., Kortesmaa, J., Cao, R., Soininen, R., Wang, L., Iivanainen, A., Sorokin, L., Risling, M., Cao, Y., and Tryggvason, K. (2002). Deletion of the laminin alpha4 chain leads to impaired microvessel maturation. Mol. Cell Biol. *22*, 1194–1202.

Timmer, J.R., Mak, T.W., Manova, K., Anderson, K.V., and Niswander, L. (2005). Tissue morphogenesis and vascular stability require the Frem2 protein, product of the mouse myelencephalic blebs gene. Proc. Natl. Acad. Sci. U S A *102*, 11746–11750.

Toda, N., Mori, K., Kasahara, M., Ishii, A., Koga, K., Ohno, S., Mori, K.P., Kato, Y., Osaki, K., Kuwabara, T., et al. (2017). Crucial role of mesangial cell-derived connective tissue growth factor in a mouse model of anti-glomerular basement membrane glomerulonephritis. Sci. Rep. *7*, 42114.

van der Wijk, A.E., Wisniewska-Kruk, J., Vogels, I.M.C., van Veen, H.A., Ip, W.F., van der Wel, N.N., van Noorden, C.J.F., Schlingemann, R.O., and Klaassen, I. (2019). Expression patterns of endothelial permeability pathways in the development of the blood-retinal barrier in mice. FASEB J. *33*, 5320–5333.

Wang, L., Luo, J.Y., Li, B., Tian, X.Y., Chen, L.J., Huang, Y., Liu, J., Deng, D., Lau, C.W., Wan, S., et al. (2016). Integrin-YAP/TAZ-JNK cascade mediates atheroprotective effect of unidirectional shear flow. Nature *540*, 579–582.

Wang, X., Freire Valls, A., Schermann, G., Shen, Y., Moya, I.M., Castro, L., Urban, S., Solecki, G.M., Winkler, F., Riedemann, L., et al. (2017). YAP/TAZ orchestrate VEGF signaling during developmental angiogenesis. Dev. Cell *42*, 462–478.e7.

Weinl, C., Castaneda Vega, S., Riehle, H., Stritt, C., Calaminus, C., Wolburg, H., Mauel, S., Breithaupt, A., Gruber, A.D., Wasylyk, B., et al. (2015). Endothelial depletion of murine SRF/MRTF provokes intracerebral hemorrhagic stroke. Proc. Natl. Acad. Sci. U S A *112*, 9914–9919.

Yasuda, D., Kobayashi, D., Akahoshi, N., Ohto-Nakanishi, T., Yoshioka, K., Takuwa, Y., Mizuno, S., Takahashi, S., and Ishii, S. (2019). Lysophosphatidic acid-induced YAP/TAZ activation promotes developmental angiogenesis by repressing Notch ligand Dll4. J. Clin. Invest. *129*, 4332–4349.

Yoshisue, H., Suzuki, K., Kawabata, A., Ohya, T., Zhao, H., Sakurada, K., Taba, Y., Sasaguri, T., Sakai, N., Yamashita, S., et al. (2002). Large scale isolation of non-uniform shear stress-responsive genes from cultured human endothelial cells through the preparation of a subtracted cDNA library. Atherosclerosis *162*, 323–334.

Zanconato, F., Forcato, M., Battilana, G., Azzolin, L., Quaranta, E., Bodega, B., Rosato, A., Bicciato, S., Cordenonsi, M., and Piccolo, S. (2015). Genome-wide association between YAP/TAZ/TEAD and AP-1 at enhancers drives oncogenic growth. Nat. Cell Biol. *17*, 1218–1227.

Zhao, B., Ye, X., Yu, J., Li, L., Li, W., Li, S., Yu, J., Lin, J.D., Wang, C.Y., Chinnaiyan, A.M., et al. (2008). TEAD mediates YAP-dependent gene induction and growth control. Genes Dev. *22*, 1962–1971.

Zhao, Z., Nelson, A.R., Betsholtz, C., and Zlokovic, B.V. (2015). Establishment and dysfunction of the blood-brain barrier. Cell *163*, 1064–1078.

iScience, Volume *23*

Supplemental Information

A CTGF-YAP Regulatory Pathway Is Essential for Angiogenesis and Barriergenesis in the Retina

Sohyun Moon, Sangmi Lee, Joy Ann Caesar, Sarah Pruchenko, Andrew Leask, James A. Knowles, Jose Sinon, and Brahim Chaqour

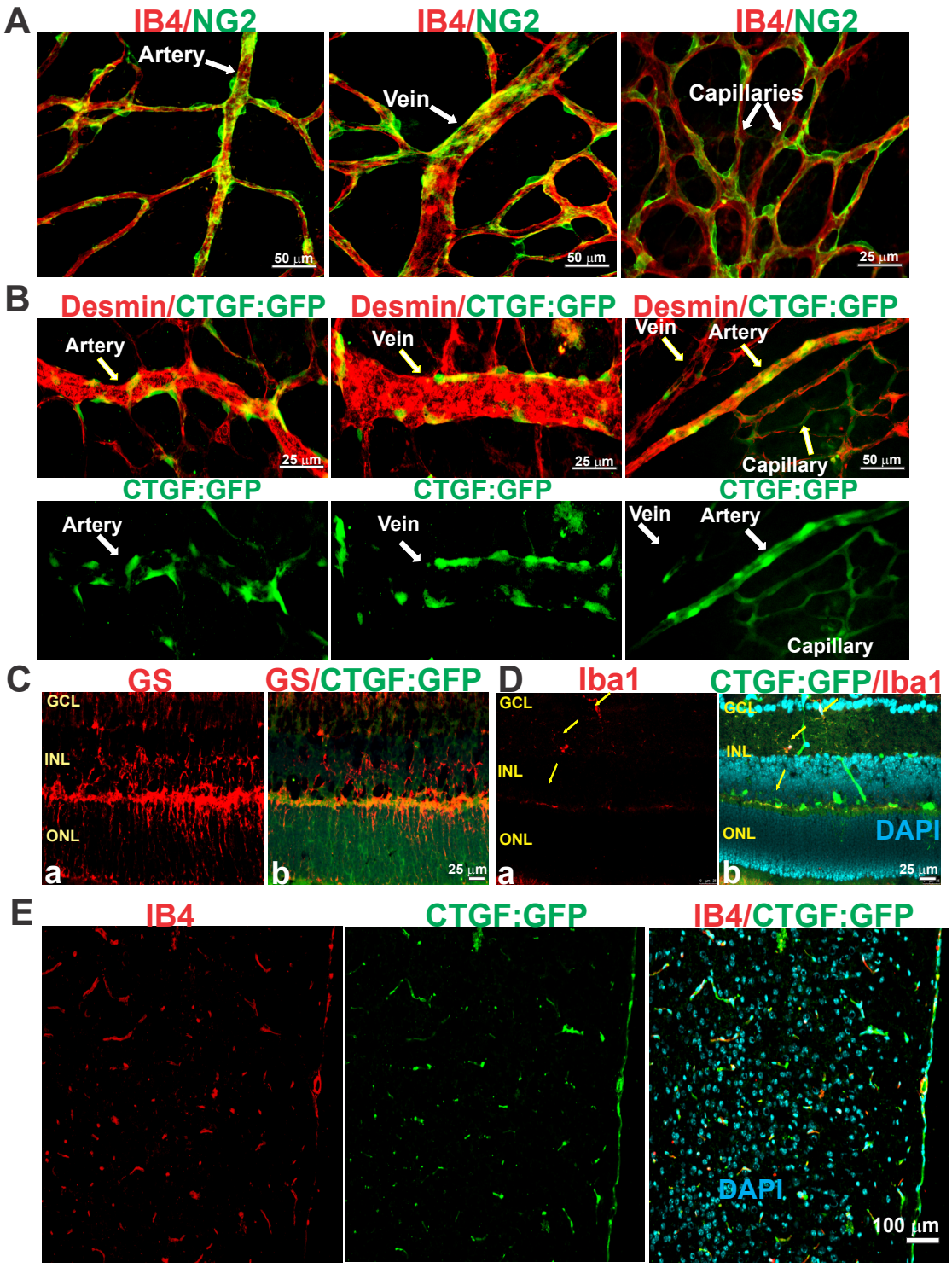

Figure S1 (related to Figure 1). Cellular Sources of CTGF in the Mouse Retinal Vasculature.

(A) Localization of the NG2 marker in IB4-stained retinal vasculature. Retinal flat mount form P7 mouse was stained with the NG2 marker. Note that arteries and capillaries expressed the NG2 marker whereas veins exhibited little or no NG2 signal.

(B) High magnification images of retinal vessels in flat-mounted retinas of the *CTGF:GFP* reporter mice showing colocalization of the GFP label with desmin staining. Note that desmin$^+$ mural cells of arteries, capillaries and veins are CTGF:GFP$^+$ as well.

(C) and (D) Transverse retinal sections from *CTGF:GFP* mice stained with either glutamine synthase (GS) and Iba1 characteristic of Müller cells and microglia, respectively. Colocalization of the GS and Iba1 markers with the GFP signal are shown in the upper panels. DAPI staining shows nuclear localization of retinal cells in the ganglion cell layer (GCL), inner nuclear layer (INL), and outer nuclear layer (ONL). Arrows indicate CTGF:GFP-Iba-1$^+$ cells.

(E) Tissue sections of P7 *CTGF:GFP* mouse brain labeled with IB4 (red for blood vessels). Colocalization of the CTGF:GFP signal with IB4+ blood vessels is shown in the merged image.

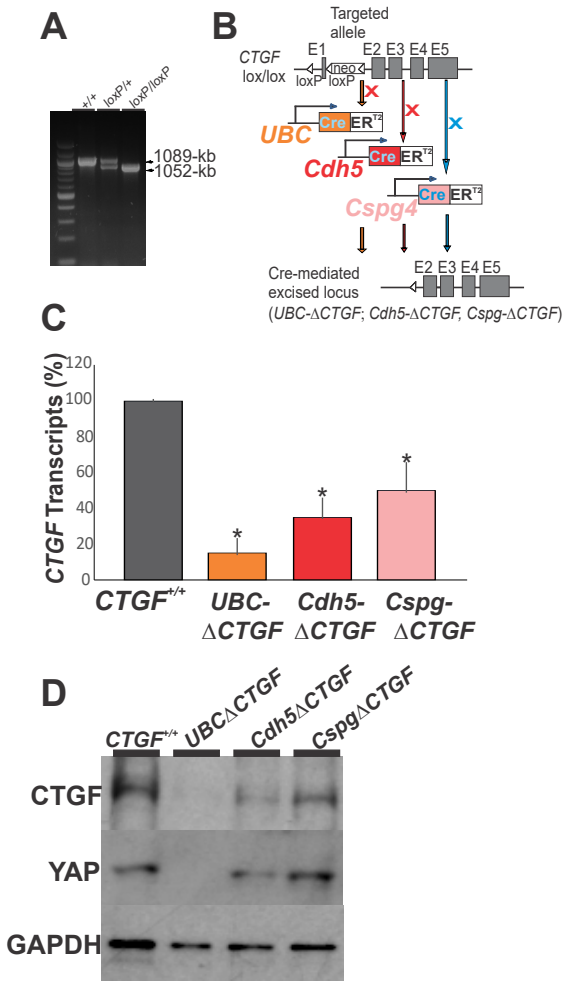

Figure S2 (related to Figure 2). Targeting of the *CTGF* Genomic Locus and Recombination in UBC-CreER^{T2}, Cdh5(PAC)-CreER^{T2} and Cspg4-CreER^{T2} Mice

(A) *CTGF* wild-type allele was detected by PCR as a 1052-bp DNA band. The floxed allele was confirmed by the presence of a 1089-bp DNA band.

(B) Schematic diagrams showing the targeted *CTGF* genomic locus with the *CTGF* flox-neo allele, the *CTGF* flox allele with the neomycin resistance cassette deleted by recombination performed with loxP sites, and the mutant locus following 4HT-induced UBC-, Cdh5 or Cspg4 promoter Cre-mediated excision.

(C) Relative *CTGF* mRNA levels in retinal lysates from *CTGF*$^{+/+}$, UBCΔ*CTGF*, Cdh5Δ*CTGF*, and CspgΔ*CTGF*. Total RNA was extracted from the whole retinal tissue and mRNA quantification was performed by qPCR. Each measurement was performed in triplicate (n=3). Values are means ± SE. *, p <0.01 *vs CTGF*$^{+/+}$ (n=4).

(D) CTGF protein detection by Western immunoblotting in retinal lysates from *CTGF*$^{+/+}$, UBCΔ*CTGF*, Cdh5Δ*CTGF*, and CspgΔ*CTGF* mice following consecutive daily injection of 4HT. GAPDH signal was used as a loading control.

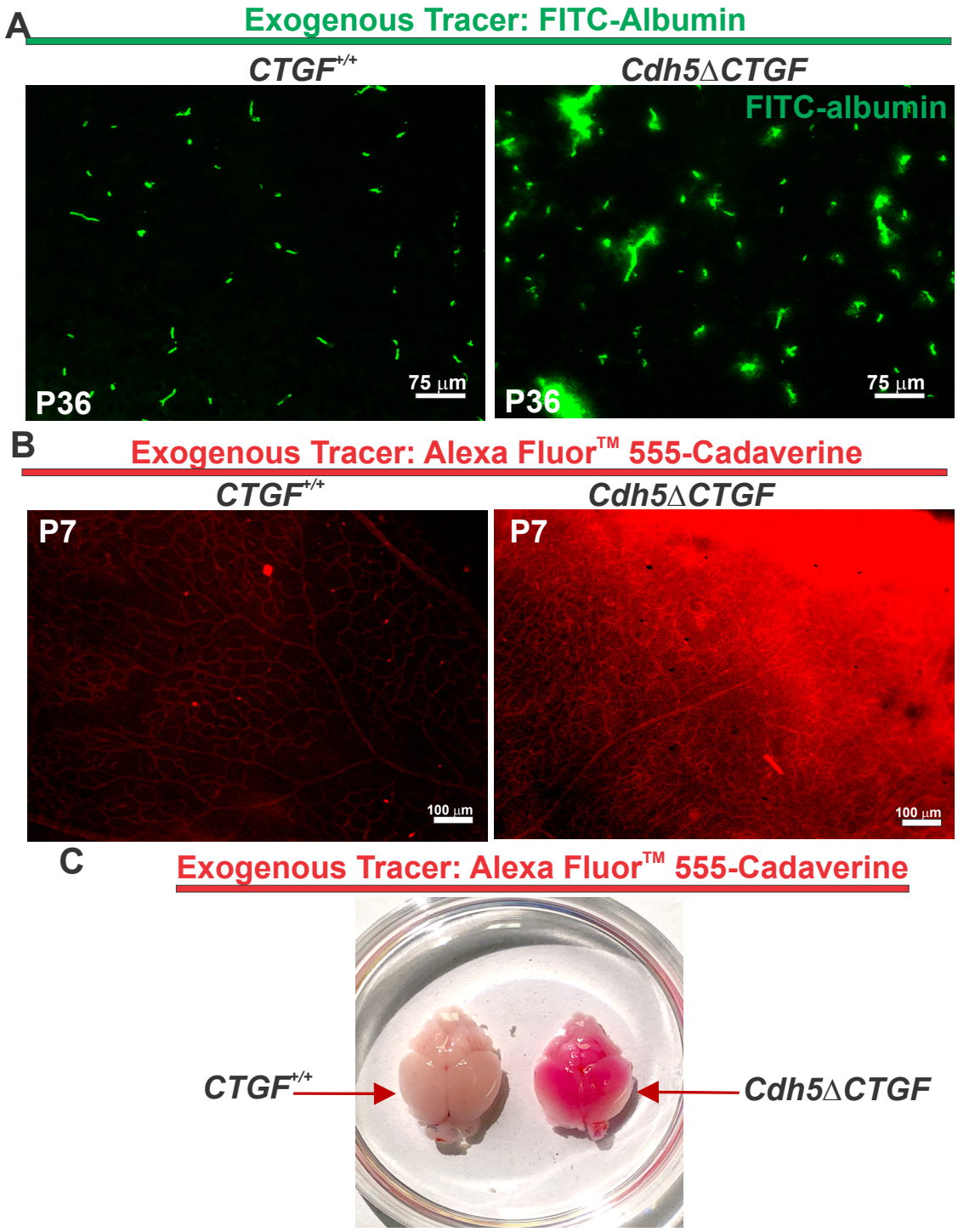

Figure S3 (related to Figure 3). Effects of *CTGF* Deletion on Blood Retina and Brain Barriers.

(A) Defective blood brain barrier in adult (P36) mice with endothelial deficiency of *CTGF*. The injected FITC-albumin tracer was confined to the capillaries in WT mice whereas the mutant mouse brain showed focal tracer leakage in the brain parenchyma surrounding capillaries in cortical areas.

(B) Representative images of retinal flat mounts from Alexa Fluor™ 555-conjugated cadaverine-injected *CTGF*$^{+/+}$ and UBCΔ*CTGF* mice at P7. Note tracer leakage and its uptake by neural cells in mutant mouse retinas.

(C) Dorsal view of *CTGF*+/+ and UBCΔ*CTGF* mutant mouse brain at P7 after injection of Alexa Fluor™ 555-conjugated cadaverine. Note the redness of mutant mouse brain cortices caused by the tracer leakage through the destabilized blood brain barrier.

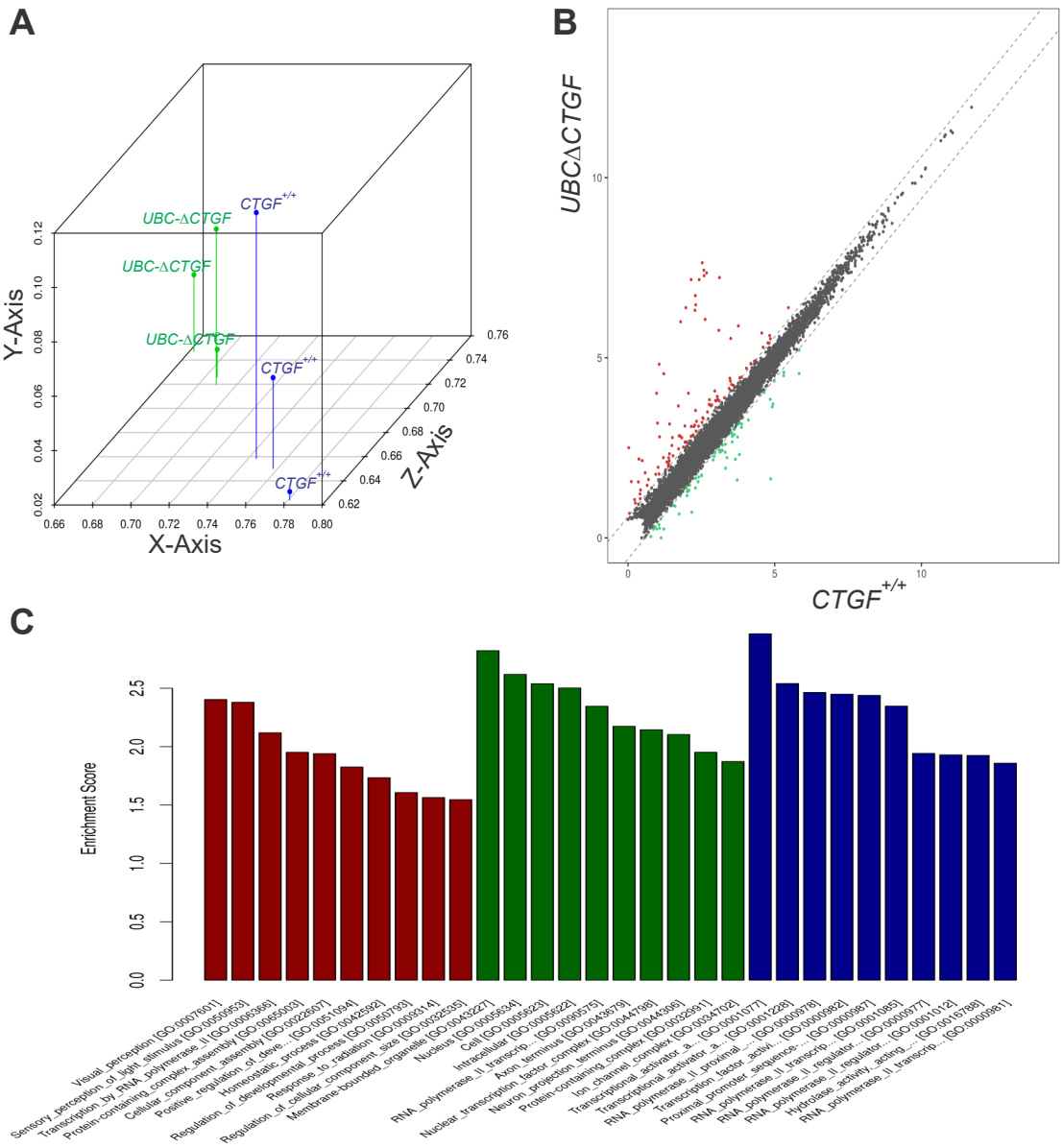

Figure S4 (related to Figure 4). Transcriptome Profiling of *CTGF*$^{+/+}$ and *UBC*Δ*CTGF* Mouse Retina at P7

(A) PCA analysis showing hallmark gene signatures with clear segregation between *CTGF*$^{+/+}$ and UBCΔ*CTGF* transcriptomes of the three biological replicates plotted in 3 D volumetric space. X-axis (52.08%), Y-axis (0.41%) and Z-axis (47.51%).

(B) Scatter plots comparing cross-sample normalized RNA Seq read counts of CTGF target genes. Red and green symbols are transcripts with false discovery rate (FDR) < 0.05 and enrichment >2 fold (values are $\log_2$ of normalized transcript counts).

(C) Top GO biological process terms enriched in up- or downregulated genes in retinas of *CTGF* mutant mice at P7.

TRANSPARENT METHODS

Mice

Animal studies were carried out in accordance with the recommendations in the Guide for the Care and Use of Laboratory Animals of the National Institutes of Health. Mice were handled and housed according to the approved Institutional Animal Care and Use Committee (IACUC) protocol 14-10425 of SUNY Downstate Medical Center. Both male and female mice were used in the study. Developmental stages are as indicated in the text. GENSAT *Tg(CTGF-EGFP)FX156Gsat*/Mmucd (011899-UCD) mice, referred to herein as *CTGF:GFP* mice carrying enhanced green fluorescent protein (GFP) under the control of the *CTGF* promoter, were developed under the NINDS-funded GENSAT BAC transgenic project (Gong et al., 2003) and obtained from the Mutant Mouse Regional Resource Center. *CTGF:GFP* mice were initially in the FVB/N-Swiss Webster background and later backcrossed for >10 times in the C57BL/6J genetic background. *CTGF*$^{flox/flox}$ were previously described (Liu et al., 2011). *Tg(UBC-cre/ER*^{T2}*)1Ejb*, *Tg(Cdh5-PAC-cre/ER*^{T2}*)* and Tg(*Cspg4-cre/ER*^{TM}) mice were from Jackson Laboratory (Ruzankina et al., 2007; Sorensen et al., 2009; Zhu et al., 2011).

See also Table S1

Generation of the CTGF conditional allele

For global and cell-specific removal of floxed STOP-cassettes, *CTGF*$^{flox/flox}$ were crossbred with *Tg(UBC-cre/ER)1Ejb*, *Tg(Cdh5-PAC-cre/ER*^{T2}) and *Tg(Cspg4-cre/ER*^{TM}*)* mice to induce global, EC-, and pericyte-specific deletion of *CTGF* respectively. Mouse genotypes were determined by PCR to identify mice with floxed alleles and hemi-and homozygous floxed alleles with or without the *Cre* allele. A solution of 4-hydroxytamoxifen (4HT) was dissolved in ethanol at 10 mg/ml, and then 4 volumes of corn oil were added. Samples of 4HT were thawed and diluted in corn oil prior to intraperitoneal injection of 100 ml to mouse pups. The relative recombination levels in mutant mice as compared with *CTGF*$^{+/+}$ were determined as previously described previously (Liu et al., 2011).

Recombinant AAV vector generation and retroorbital injection

AAV6 vectors expressing *GFP* or *YAP* cDNA under the control of the *cytomegalovirus* (*CMV*) promoter were used. *AAV6-GFP* control was obtained from the Penn Vector Core at the University of Pennsylvania. *AAV6-YAP* vector was produced by triple transfection of 293T cells with the *pAV-FH AAV* vector, the Ad helper vector, and a vector encoding the Rep and serotype-specific Cap proteins, followed by iodixanol gradient centrifugation and purification by anion-exchange chromatography. Viral titers were determined as the number of genomic copies (GC) per microliter using quantitative real-time PCR ($1x10^{12}$ GC/ml). AAV packaging, purification, and quality control were performed by Vigene Biosciences. For retroorbital injection, mouse pups were anesthetized using

ketamine/xylazine mixture prior to retro-orbital injection of the recombinant viral vectors ($4x10^{12}$ vector genomes) in 15 μl of sterile phosphate buffer solution (PBS).

Cell culture

Primary brain and aorta ECs were isolated by immunopanning from both P7 male and female WT and *UBC⊿CTGF* mice. Cells were authenticated by endothelial marker expression (CD31/DiI-acLDL double-positive) and morphology. Cells were cultured in endothelial medium supplemented with 10% fetal bovine serum (FBS) to promote formation of confluent monolayer cultures. All cell cultures were used between passage 3 to 9.

Adenoviral vector infection

Mouse *YAP* cDNAs were isolated by PCR amplification using DNA templates obtained from Addgene (Watertown, MA) and cloned into a shuttle vector at Creative-Biogene (Shirley, NY). The recombinant adenovirus, *Ad-YAP*, was produced by cotransfecting an adenoviral shuttle vector with a viral backbone in which the recombinant cDNA is driven by the *CMV* promoter. All adenoviruses were replication-deficient and used at 20 multiplicity of infection to transduce cultured ECs. Adenoviral vectors were added to ECs cultured in medium containing 2% FBS and incubated for 4 h. Thereafter, the cells were washed five times and cultured in medium with 10% FBS and supplements. The adenovirus encoding the luciferase gene, Ad-Luc (obtained from the Gene Therapy Resource Program Vector Core Laboratory at the University of Pennsylvania) was used as a control.

Quantification of junctional density, length, and lacunarity of retinal vessels

Mouse eyes were collected at the indicated postnatal days and fixed in 4% paraformaldehyde (PFA) for 2 h. Retinas were dissected and laid flat on SuperFrost^{R} Plus-coated slides, permeabilized in 0.1% Triton X-100 at room temperature and stained with IB4, as previously described (Lee et al., 2017). Fields of view of the retinal vascular networks from control and mutant mice were captured by using the x2 and x40 objective lenses. Using AngioTool (Zudaire et al., 2011), vascular parameters such as total vascular surface area, vessel junctional density and “gappiness”/lacunarity of the vascular network were determined. For each parameter, at least four fluorescent images/retina were taken from 3–5 mice. The data are presented as means $\pm$SE. The statistical significance of differences among mean values was determined by one-way analysis of variance and two-tailed *t* test.

Immunohistochemical staining

Eyes were frozen in Tissue-Tek Optimal Cutting temperature compound and five to ten micrometer-thick cryostat sections were prepared. Retinas dissected from different sets

of eyes were laid flat on SuperFrost® Plus coated slides to obtain whole mount preparations. Sections and flat mounted preparations were then permeabilized in 0.1% Triton X-100 at room temperature for 20 min and further single odouble stained with IB4 and/or with primary antibodies as indicated in Table S1. Immunodetection was performed with either rhodamine or fluorescein-conjugated anti-mouse or anti-rabbit secondary antibody diluted in blocking solution. Retinal mounts and sections were mounted in 4′,6-diamidino-2-phenylindole (DAPI). Images were acquired using a Leica DM5500B fluorescence microscope (Leica). To localize proteins in cultured cells, cells were fixed in PFA for 10 min and permeabilized in 0.1% Triton X-100 at room temperature for 5 min. Cells were then incubated with the indicated primary antibodies (e.g., ZO-1, YAP (Cell Signaling, 1:250) overnight at 4 °C and treated with TRITC- or FITC-conjugated secondary antibodies. Cytoskeletal actin was visualized using Phalloidin (Cytoskeleton Inc.). Images were captured using a Leica DM5000 B fluorescence imaging system.

BrdU incorporation and cell proliferation assay

WT and *CTGF* mutant mice was intraperitoneally injected with 100 μl of 3 μg/ml BrdU per 3 g body weight. For BrdU labeling, retinas were digested with Proteinase K (10 μg/ml), fixed in 4% PFA, treated with DNase I (0.1 units/ml) for 2 h at 37 °C, and incubated with anti-BrdU antibody (1: 50, BD Pharmingen). ECs were visualized by staining with IB4 (Molecular Probes), and BrdU was detected using conjugated mouse anti-BrdU Alexa 488 (Molecular Probes). $BrdU^+$ cells that co-localized in ECs at the vascular front were counted, and numbers of $BrdU^+$ cells were normalized to the vessel area or vessel length determined by AngioTool. The sum of $BrdU^+$ cells for the four leaflets of the retina was normalized to the sum of analyzed vessel area for each animal. For cultured cells, proliferation rate was determined using the CyQUANT Direct Cell Proliferation Assay according to the manufacturer's protocol (Invitrogen). The fluorescence intensity was measured with a fluorescence microplate reader using an FITC filter set.

In vivo permeability assays

Vascular permeability was determined using the highly sensitive FITC-albumin permeability assay. Anesthetized mice received retro-orbital injections of 50 μl of 1% albumin-AlexaFluor 488 (Sigma-Aldrich). After 5 min, animals were sacrificed, and the eyes were enucleated and fixed in PFA for 10 min. Retinas were dissected from the eyewall and optic nerve and FITC-albumin was immediately visualized with a Leica 65700 fluorescence microscope. Retinas were further stained with IB4 and analyzed using DFM software. The area of albumin present in the retina was normalized to that of total vascular areas. For quantitative analysis of the vascular barrier leakage, anesthetized mice received intraperitoneal injections of 100 μl of EB (45 mg/kg). Enucleated retinas were harvested, homogenized and incubated in formamide for 24 hours at 55°C for EB extraction as previously described (Huynh et al., 2011). Supernatants were collected and

the absorbance of 620 nm was measured. The concentration of dye in the extracts was calculated using a standard curve.

RNA isolation and RT-qPCR

Total RNA was extracted from mouse retina using TRIzol reagent (Sigma). The cDNA synthesis was carried out by using Prime script reverse transcript kit (Takara). Highly specific primers were designed using Web-based primer design programs. A qPCR was performed with biological triplicates using Power SYBR^{TM} green PCR premix (Applied biosystems). The cycling parameters for qPCR amplification reactions were: AmpliTaq activation at 95°C for 10min, denaturation at 95°C for 15s, and annealing/extension at 60°C for 1min (40 cycles). Triplicate *Ct* values were analyzed with Microsoft Excel using the comparative *Ct* ($\Delta\Delta^{Ct}$) method as described by the manufacturer. The transcript amount (determined by the $-2^{\Delta\Delta Ct}$ threshold cycle [C_T] method) was obtained by normalizing to an endogenous reference (18S rRNA) relative to a calibrator.

Library preparation for Illumina sequencing

Retinas were harvested from *CTGF*$^{+/+}$ and *UBC⊿CTGF* at P7 (3 replicates from each control and mutant mice originating from different litters). Total RNA was extracted using TRizol. 1~2 mg total RNA of each sample was used for RNA-seq library preparation. RNA-Seq analysis was performed by Arraystar (USA). Briefly, mRNA was isolated from total RNA with NEBNext® Poly(A) mRNA Magnetic Isolation Module. The enriched mRNA was used for RNA-Seq library preparation using KAPA Stranded RNA-Seq Library Prep Kit (Illumina). Library preparation procedure included (a), fragmentation of the RNA molecules; (b) reverse transcription to synthesize first strand cDNA; (c) second strand cDNA synthesis incorporating dUTP; (d) end-repair and A-tailing of the double stranded cDNA; (e) Illumina compatible adapter ligation; and (f) PCR amplification and purification for the final RNA-Seq library. The completed libraries were qualified on an Agilent 2100 Bioanalyzer for concentration, fragment size distribution between 400 ~ 600 bp, and adapter dimer contamination. The amount was determined by the absolute quantification qPCR method. The bar-coded libraries were mixed in equal amounts and used for sequencing. The DNA fragments in well mixed libraries were denatured with 0.1M NaOH to generate single-stranded DNA molecules, loaded onto channels of the flow cell at 8 pM concentration, and amplified *in situ* using TruSeq SR Cluster Kit v3-cBot-HS (#GD-401-3001, Illumina). Sequencing was carried out using the Illumina HiSeq 4000 according to the manufacturer's instructions. Sequencing was carried out by running 150 cycles.

Filtering and merging of reads

Image analysis and base calling were performed using Solexa pipeline v1.8 (Off-Line Base Caller software, v1.8). Sequence quality was examined using the FastQC software. The trimmed reads (trimmed 5',3'-adaptor bases using Cutadapt) were aligned to

reference genome using Hisat2 software (v2.0.4) (Kim et al., 2015). The transcript abundance for each sample was estimated with StringTie (v1.2.3) (Pertea et al., 2015), and the Fragments Per Kilobase of transcript per Million mapped (FPKM) value (Mortazavi et al., 2008) for gene and transcript levels were calculated with R package Ballgown (v2.6.0) (Frazee et al., 2015). The thresholds used for identifying differentially expressed genes (DEGS) were: (i) DESeq. 2 mean normalized counts >10; (ii) padj-value <0.5, and (iii) $\log_2$fold change >0 (Love et al., 2014). rMATS (Shen et al., 2014) was used to analyze alternative splicing events.

Pathways analysis

The differentially expressed genes/transcripts were analyzed for their enrichment in gene ontological functions or pathways using the TopGo R software package. The statistical significance of enrichment was given as p-value by Fisher exact test and $-\log_{10}(p)$ transformed to Enrichment score. Principal Component Analysis (PCA) was performed with genes that have the ANOVA p value < 0.05 on FPKM abundance estimations. Statistical or graphics computing, correlation analysis, Hierarchical Clustering, scatter plots and volcano plots were performed in R, Python or shell environment. The raw RNA-Seq data and analyzed FPKM values can be accessed through NCBI/GEO (GSE146900).

Gene set enrichment analysis

RNA-Seq dataset expression of gene profiling files downloaded from the dataset was analyzed by Gene Set Enrichment Analysis (GSEA, http://www.broad.mit.edu/gsea/index.html). Gene sets are available from Molecular Signatures DataBase (MolSigDB, http://www.broad.mit.edu/gsea/.msigdb/msigdb_index.html). The whole genome (27455 genes) with expression values were uploaded to the software and compared with catalog C5 gene ontology gene sets in MsigDB (Subramanian et al., 2005), which contains 233 GO cellular component gene sets, 825 GO biological process gene sets, and 396 GO molecular function gene sets. GSEA was run according to default parameters: collapses each probe set into a single gene vector (identified by its HUGO gene symbol), permutation number = 1000, and permutation type = “gene-sets”. Calculation of the false discovery rate (FDR) was used to correct for multiple comparisons and gene set sizes. Heat maps were generated using GENE-E, from the Broad Institute (http://www.broadinstitute.org/cancer/software/GENE-E/) for the *CTGF* and *YAP* transcriptomes.

Western immunoblotting

For protein analysis from retinas, mouse eyes were enucleated and retinas were carefully dissected and homogenized in lysis buffer containing 10 mM NaF, 300 mM NaCl, 50 mM Tris, pH 7.4, 1% Triton X-100, 10% glycerol, and 1mM EDTA with a 1% volume of

phosphatase and protease inhibitor mixture. Protein samples (20 μg) were fractioned in a 10% SDS-polyacrylamide gel, transferred to a nitrocellulose membrane, and Western blot analysis was performed with the primary antibodies indicated in the text. Immunodetection was performed using enhanced chemiluminescence (Pierce). Protein bands were quantified by densitometric scanning. To analyze proteins from cell cultures, cells were homogenized in lysis buffer fractioned by electrophoresis and analyzed as described above. The primary antibodies used in this study were for pYAP, YAP, GAPDH and CTGF. CTGF antibody (1:500) were generated using two 16-amino acid peptides (residues between 179 and 195 in the primary sequence of the mouse *CTGF*, GenBank accession no. NM_010217) was synthesized and purified by high-performance liquid chromatography (Biosynthesis). Antibodies were raised against KLH-coupled peptide in rabbits by Pocono Rabbit Farm and Laboratory Inc (Poconos, PA). After completion of the immunization process, the rabbits were exsanguinated, and the antibodies were purified by affinity chromatography using affinity columns. Bound antibodies were eluted with 100 mM glycine and immediately neutralized with Tris base and adjusted to a concentration of 0.4 mg/ml before storage at -20°C. Serum titer was determined by enzyme-linked immunosorbent assay.

Immunoprecipitation

Total proteins (~10 mg) of cultured cell lysates were transferred to tubes with antibody-bound protein G beads and rocked gently at 4°C overnight. Non-specific bound proteins were removed with five washes with 1× PBS containing 1% NP-40. Immunoprecipitation products were extracted from the protein G beads using sample loading buffer and were further analyzed by Western immunoblotting.

Statistical Analyses

Data were expressed as means ± SE. To test differences among several means for significance, a one way analysis of variance with the Newman-Keuls multiple comparison test was used. Where appropriate, a *post hoc* unpaired *t* test was used to compare two means/groups. Non-parametric Mann-Whitney or Kruskal-Wallis test was used when data collected do not have normal or clear distribution. Statistical significance was set to *p* value less than 0.05.

REFERENCES **(For Transparent Methods)**

Frazee, A.C., Pertea, G., Jaffe, A.E., Langmead, B., Salzberg, S.L., and Leek, J.T. (2015). Ballgown bridges the gap between transcriptome assembly and expression analysis. Nat Biotechnol *33*, 243-246.

Gong, S., Zheng, C., Doughty, M.L., Losos, K., Didkovsky, N., Schambra, U.B., Nowak, N.J., Joyner, A., Leblanc, G., Hatten, M.E.*, et al.* (2003). A gene expression atlas of the central nervous system based on bacterial artificial chromosomes. Nature *425*, 917-925.
Huynh, J., Nishimura, N., Rana, K., Peloquin, J.M., Califano, J.P., Montague, C.R., King, M.R., Schaffer, C.B., and Reinhart-King, C.A. (2011). Age-related intimal stiffening enhances endothelial permeability and leukocyte transmigration. Sci Transl Med *3*, 112ra122.
Kim, D., Langmead, B., and Salzberg, S.L. (2015). HISAT: a fast spliced aligner with low memory requirements. Nat Methods *12*, 357-360.
Lee, S., Elaskandrany, M., Ahad, A., and Chaqour, B. (2017). Analysis of CCN Protein Expression and Activities in Vasoproliferative Retinopathies. Methods Mol Biol *1489*, 543-556.
Liu, S., Shi-wen, X., Abraham, D.J., and Leask, A. (2011). CCN2 is required for bleomycin-induced skin fibrosis in mice. Arthritis Rheum *63*, 239-246.
Love, M.I., Huber, W., and Anders, S. (2014). Moderated estimation of fold change and dispersion for RNA-seq data with DESeq2. Genome Biol *15*, 550.
Mortazavi, A., Williams, B.A., McCue, K., Schaeffer, L., and Wold, B. (2008). Mapping and quantifying mammalian transcriptomes by RNA-Seq. Nat Methods *5*, 621-628.
Pertea, M., Pertea, G.M., Antonescu, C.M., Chang, T.C., Mendell, J.T., and Salzberg, S.L. (2015). StringTie enables improved reconstruction of a transcriptome from RNA-seq reads. Nat Biotechnol *33*, 290-295.
Ruzankina, Y., Pinzon-Guzman, C., Asare, A., Ong, T., Pontano, L., Cotsarelis, G., Zediak, V.P., Velez, M., Bhandoola, A., and Brown, E.J. (2007). Deletion of the developmentally essential gene ATR in adult mice leads to age-related phenotypes and stem cell loss. Cell Stem Cell *1*, 113-126.
Shen, S., Park, J.W., Lu, Z.X., Lin, L., Henry, M.D., Wu, Y.N., Zhou, Q., and Xing, Y. (2014). rMATS: robust and flexible detection of differential alternative splicing from replicate RNA-Seq data. Proc Natl Acad Sci U S A *111*, E5593-5601.
Sorensen, I., Adams, R.H., and Gossler, A. (2009). DLL1-mediated Notch activation regulates endothelial identity in mouse fetal arteries. Blood *113*, 5680-5688.
Subramanian, A., Tamayo, P., Mootha, V.K., Mukherjee, S., Ebert, B.L., Gillette, M.A., Paulovich, A., Pomeroy, S.L., Golub, T.R., Lander, E.S.*, et al.* (2005). Gene set enrichment analysis: a knowledge-based approach for interpreting genome-wide expression profiles. Proc Natl Acad Sci U S A *102*, 15545-15550.
Zhu, X., Hill, R.A., Dietrich, D., Komitova, M., Suzuki, R., and Nishiyama, A. (2011). Age-dependent fate and lineage restriction of single NG2 cells. Development *138*, 745-753.
Zudaire, E., Gambardella, L., Kurcz, C., and Vermeren, S. (2011). A computational tool for quantitative analysis of vascular networks. PLoS One *6*, e27385.

Table S1: Key Resources (related to Transparent Methods)

REAGENTS or RESOURCE	SOURCE	IDENTIFER
Experimental Models: Mice		
Tg(Ctgf-EGFP)FX156Gsat/Mmucd	MMRRC	011899-UCD
CTGF$^{flox/flox}$	Liu et al, 2011	N/A
Tg(UBC-cre/ER^{T2})1Ejb	Jackson Labs	007001
Tg(Cdh5-PAC-cre/ER^{T2})	Sorensen et al, 2009	N/A
*Tg(*Cspg4-cre/ER^{TM}	Jackson Labs	008538
Experimental Models: Cells		
Brain ECs	This paper	N/A
Recombinant viruses		
AAV6-*GFP*	*GTRP-U Penn*	N/A
AAV6-*luc*	*GTRP-U Penn*	N/A
AAV6-*YAP*	*Vigene Bioscience*	N/A
Ad-*luc*	*GTRP-U Penn*	N/A
Ad-*YAP*	*Creative-Biogene*	N/A
Antibodies		
Collagen IV	Millipore Sigma	Cat# AB756P
Iba-1	Wako	Cat# 019-19741
NG2	Millipore Sigma	Cat# MAB5384
Desmin	Dako	Cat# M0760
ZO-1	Invitrogen	Cat# 61-7300
Phospho YAP (Ser127)	Cell signaling	Cat# 4911
YAP	Santa Cruz	Cat# sc-101199
CDH5 (VE-Cadherin)	Santa Cruz	Cat# sc-9989
pTyr731 CDH5	Millipore	Cat# AB1956
Alpha-catenin	Abcam	Cat# Ab51032
Glutamine synthase	Millipore	Cat# MAB302
Conjugated mouse IgG	Cell signaling	Cat# 7076S
Conjugated rabbit IgG	Cell signaling	Cat# 7074S
Deposited data		
Raw and analyzed RNA-Seq data	This paper	GEO: GSE146900
Chemicals		

Isolectin B4	Vector Laboratories	Cat# DL-1207
DAPI	Millipore Sigma	Cat# F6057
FITC-albumin	Millipore Sigma	Cat# A9771
Alexa Fluor555-conjugated cadaverine	Invitrogen	Cat# A30677
Phalloidin	Cytoskeleton	Cat# PHDR1
Software and Algorithms		
Angiotool	Zudaire et al, 2011	N/A
Hisat2 software	Kim et al, 2015a	N/A
StringTie	Pertea et al, 2015	N/A
Ballgown R package	Frazee et al., 2015	N/A